

Journal Pre-proofs

Discovery of amide-bridged pyrrolo[2,3-*d*]pyrimidines as tumor targeted classical antifolates with selective uptake by folate receptor α and inhibition of *de novo* purine nucleotide biosynthesis

Weiguo Xiang, Aamod Dekhne, Arpit Doshi, Carrie O'Connor, Zhanjun Hou, Larry H. Matherly, Aleem Gangjee

PII: S0968-0896(19)31111-3
DOI: <https://doi.org/10.1016/j.bmc.2019.115125>
Reference: BMC 115125



To appear in: *Bioorganic & Medicinal Chemistry*

Received Date: 1 July 2019
Accepted Date: 17 September 2019

Please cite this article as: Xiang, W., Dekhne, A., Doshi, A., O'Connor, C., Hou, Z., Matherly, L.H., Gangjee, A., Discovery of amide-bridged pyrrolo[2,3-*d*]pyrimidines as tumor targeted classical antifolates with selective uptake by folate receptor α and inhibition of *de novo* purine nucleotide biosynthesis, *Bioorganic & Medicinal Chemistry* (2019), doi: <https://doi.org/10.1016/j.bmc.2019.115125>

This is a PDF file of an article that has undergone enhancements after acceptance, such as the addition of a cover page and metadata, and formatting for readability, but it is not yet the definitive version of record. This version will undergo additional copyediting, typesetting and review before it is published in its final form, but we are providing this version to give early visibility of the article. Please note that, during the production process, errors may be discovered which could affect the content, and all legal disclaimers that apply to the journal pertain.

Discovery of amide-bridged pyrrolo[2,3-*d*]pyrimidines as tumor targeted classical antifolates with selective uptake by folate receptor α and inhibition of *de novo* purine nucleotide biosynthesis

Weiguo Xiang[£], Aamod Dekhne[‡], Arpit Doshi[£], Carrie O'Connor[‡], Zhanjun Hou^{‡ll},

Larry H. Matherly^{‡§ll£*}, Aleem Gangjee^{££*}

^{£*}Division of Medicinal Chemistry, Graduate School of Pharmaceutical Sciences, Duquesne University, 600 Forbes Avenue, Pittsburgh, PA 15282

^{ll}Molecular Therapeutics Program, Barbara Ann Karmanos Cancer Institute, 421 E. Canfield Street, Detroit, MI 48201

[‡]Department of Oncology, Wayne State University School of Medicine, Detroit, MI 48201

[§]Department of Pharmacology, Wayne State University School of Medicine, Detroit, MI 48201

[£]These authors contributed equally to this work.

*To whom correspondence should be addressed.

AUTHOR INFORMATION

Corresponding Authors

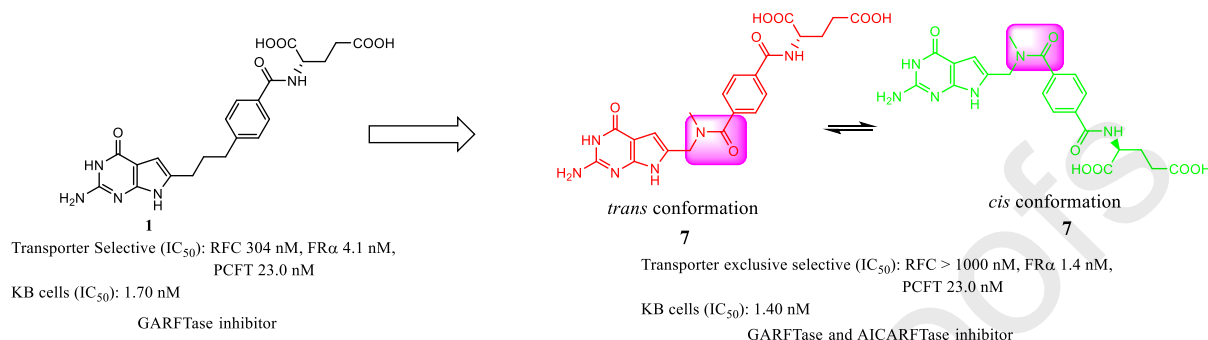
Aleem Gangjee, Ph.D., Division of Medicinal Chemistry, Graduate School of Pharmaceutical Sciences, Duquesne University, 600 Forbes Avenue, Pittsburgh, PA 15282. Phone: 412-396-6070; fax: 412-396-5593; gangjee@duq.edu

Larry H. Matherly, Ph.D., Molecular Therapeutics Program, Barbara Ann Karmanos Cancer Institute, 421 East Canfield Street, Detroit, MI 48201. Phone: 313-578-4280; fax: 313-578-4287; matherly@karmanos.org

Keywords: classical antifolates; folate receptor; selective uptake; pyrrolo[2,3-*d*]pyrimidines, amide bridge

Abbreviations used:

FR, Folate Receptor; GAR, Glycinamide Ribonucleotide; GARFTase, Glycinamide Ribonucleotide Formyltransferase; RFC, Reduced Folate Carrier; AICA, 5-Aminoimidazole-4-Carboxamide; AICARFTase, 5-Aminoimidazole-4-Carboxamide Ribonucleotide Formyltransferase; MTX, Methotrexate; PDX, Pralatrexate; RTX, Raltitrexed; PMX, Pemetrexed; PCFT, Proton-Coupled Folate Transporter



Abstract

We previously showed that classical 6-substituted pyrrolo[2,3-*d*]pyrimidine antifolates bind to folate receptor (FR) α and the target purine biosynthetic enzyme glycylamide ribonucleotide formyltransferase (GARFTase) with different *cis* and *trans* conformations. In this study, we designed novel analogs of this series with an amide moiety in the bridge region that can adopt both the *cis* and *trans* lowest energy conformations. This provides entropic benefit, by restricting the number of side-chain conformations of the unbound ligand to those most likely to promote binding to FR α and the target enzyme required for antitumor activity. NMR of the most active compound **7** showed both *cis* and *trans* amide bridge conformations in ~1:1 ratio. The bridge amide group in the best docked poses of **7** in the crystal structures of FR α and GARFTase adopted both *cis* and *trans* conformations, with the lowest energy conformations predicted by Maestro and evidenced by NMR within 1 kcal/mol. Compound **7** showed ~3-fold increased inhibition of FR α -expressing cells over its non-restricted parent analog **1** and was selectively internalized by FR α over the reduced folate carrier (RFC), resulting in significant *in vitro* antitumor activity toward FR α -expressing KB human tumor cells. Antitumor activity of **7** was abolished by treating cells

with adenosine but was incompletely protected by 5-aminoimidazole-4-carboxamide (AICA) at higher drug concentrations, suggesting GARFTase and AICA ribonucleotide formyltransferase (AICARFTase) in *de novo* purine biosynthesis as the likely intracellular targets. GARFTase inhibition by compound **7** was confirmed by an *in situ* cell-based activity assay. Our results identify a “first-in-class” classical antifolate with a novel amide linkage between the scaffold and the side chain aryl L-glutamate that affords exclusive selectivity for transport *via* FR α over RFC and antitumor activity resulting from inhibition of GARFTase and likely AICARFTase. Compound **7** offers significant advantages over clinically used inhibitors of this class that are transported by the ubiquitous RFC, resulting in dose-limiting toxicities.

1. INTRODUCTION

Antifolates that inhibit one-carbon biosynthetic enzymes such as dihydrofolate reductase and thymidylate synthase are important agents for anticancer chemotherapy.^{1,2} Clinically useful antifolates include methotrexate (MTX), pralatrexate (PDX), raltitrexed (RTX) and pemetrexed (PMX) (**Figure 1**) with applications for both hematologic malignancies and solid tumors.² Unfortunately, dose-limiting toxicities plague the clinical utility of these drugs and are due, at least in part, to non-specific drug accumulation resulting in inhibition of critical enzyme targets and downstream pathways in both tumors and normal tissues without selectivity.

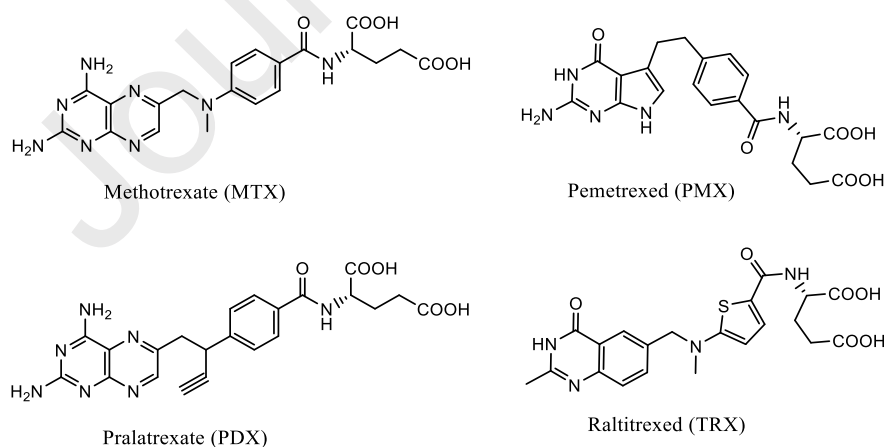


Figure 1. Clinically used antifolate drugs for cancer.

The principal (anti)folate transport system in tissues and tumors is the ubiquitously expressed reduced folate carrier (RFC).³ Notably, all the aforementioned antifolates (**Figure 1**) are excellent substrates for transport by RFC and accumulate in normal tissues, as well as in tumor cells, precluding selectivity.^{1,3} Uptake systems with greater tumor specificity than RFC have been described and include the proton-coupled folate transporter (PCFT)⁴⁻⁷ and folate receptor (FR) α .^{8,9} PCFT is a proton symporter that is expressed in a wide range of solid tumors, including ovarian cancer, non-small cell lung cancer, and malignant pleural mesothelioma.¹⁰⁻¹³ Moreover, PCFT is active at acidic pH characterizing the microenvironments of solid tumors.^{6,14} Although certain normal tissues such as the proximal small intestine, liver, and kidney also express PCFT, the tissue microenvironments of most normal tissues are unlikely to be sufficiently acidic to support PCFT transport,⁷ except the jejunum where the pH is acidic and conducive of folate transport.

FR α is expressed on the surface of epithelial ovarian, non-small cell lung, kidney, endometrial, colorectal and breast cancers where it comes into contact with the systemic circulation.^{8,9,15} FR α is also expressed in a subset of normal tissues including kidney, lung, choroid plexus and placenta. However, in contrast to tumors, in normal tissues, FR α localizes to the luminal membranes without exposure to the systemic circulation.^{8,9,15} Thus, there is a compelling rationale for developing FR- and PCFT-based therapies for cancer, particularly for solid tumors.

Clinically tested FR α -targeted therapies include a FR α monoclonal antibody [Farletuzumab (Morphotech)^{16,17}], a FR α -targeting antibody-drug conjugate [IMGN853 (ImmunoGen)¹⁸], and cytotoxic folic acid (FA) conjugates [Vintafolide, EC1456 and EC1788 (Endocyte)]^{9,19}. Although an FR-targeted antifolate *N*-[4-[2-propyn-1-yl]-(6*S*)-4,6,7,8-tetrahydro-2-(hydroxymethyl)-4-oxo-3*H*-cyclopenta[g]quinazolin-6-yl] amino benzoyl]-L- γ -glutamyl-D-glutamic acid (ONX0801) was described^{20,21} and advanced to a phase 1 clinical trial,²² no FR α -targeted antifolate has yet been FDA-approved for cancer.

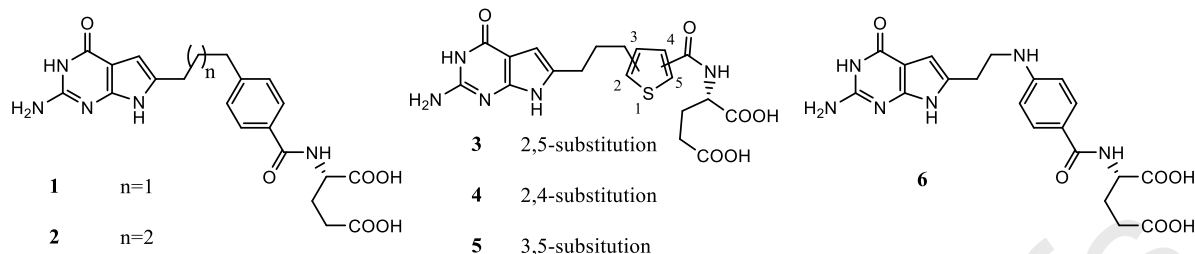
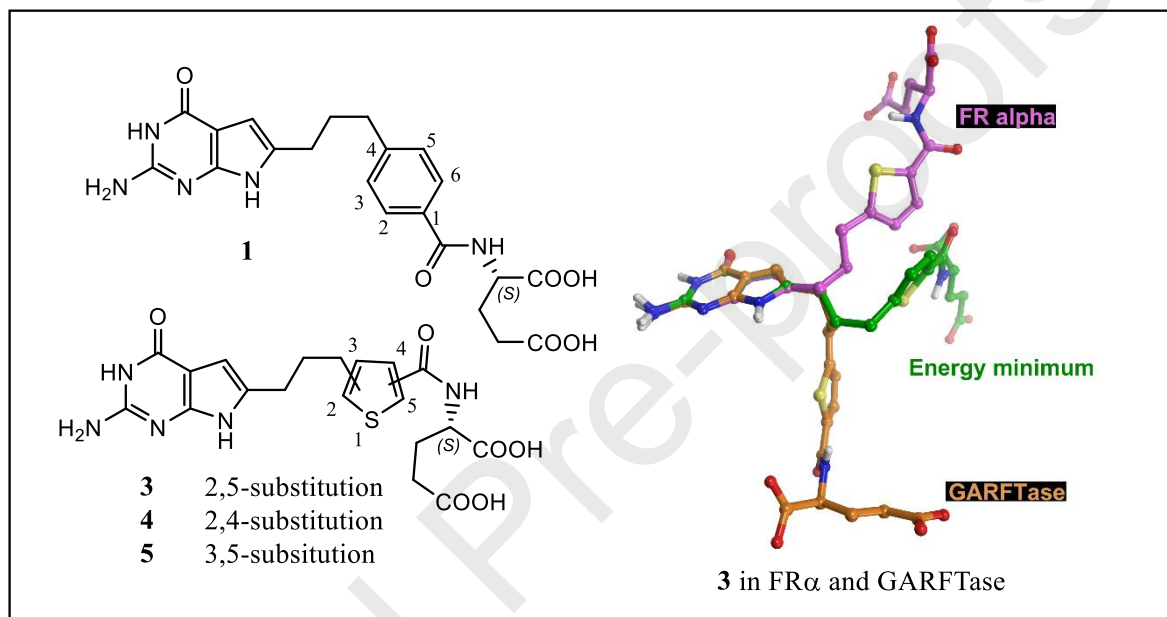


Figure 2. 6-Substituted pyrrolo[2,3-*d*]pyrimidine antifolates **1-6**.

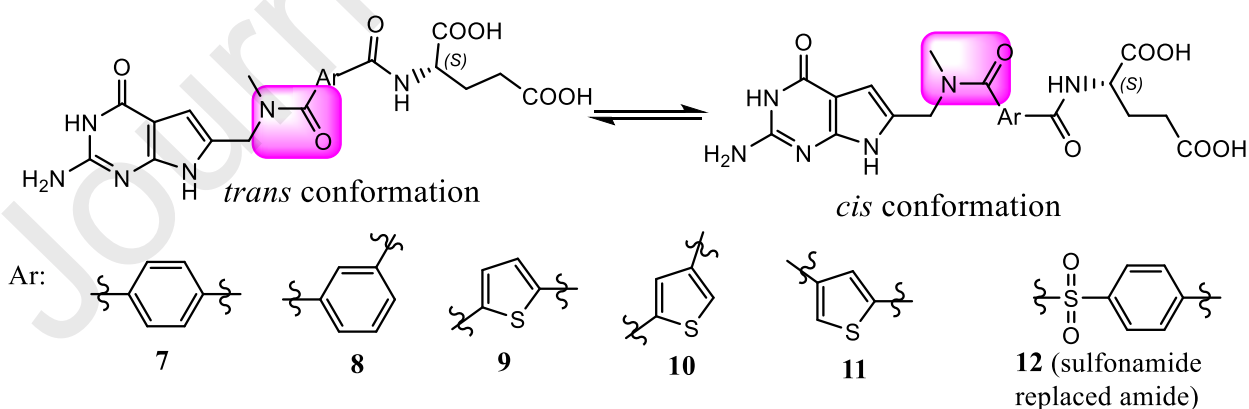
We discovered novel 6-substituted pyrrolo[2,3-*d*]pyrimidine benzoyl *L*-glutamate antifolates with 3- or 4-bridge carbons (CH_2) (**1** and **2**, respectively) (**Figure 2**) as selective transport substrates for FRs and/or PCFT over RFC.^{23,24} Following internalization by tumor cells, these compounds inhibited glycinamide ribonucleotide (GAR) formyltransferase (GARFTase), the first folate-dependent step in *de novo* purine biosynthesis. Side-chain replacement of the phenyl moiety of **1** with thienyl regioisomers (**3-5**) (**Figure 2**) increased the inhibitory effects toward FR α -expressing cells and with PCFT-expressing cells, as well.^{25,26} *N*-heteroatom substitution in the bridge region as in **6** (**Figure 2**) increased FR α -targeting at the expense of RFC and PCFT uptake; however, **6** did not show absolute selectivity for FR or PCFT over RFC.²⁷

Cytotoxic drugs generally bind to different cellular targets in distinct conformations. For anionic compounds, a requisite step in drug activity involves mediated uptake into tumor cells (ideally via a tumor-selective uptake process), whereupon they inhibit intracellular target enzymes. In principle, these compounds could adopt distinct conformations, including one that strongly favors mediated uptake into cells and another favoring binding to an intracellular enzyme target(s) that ultimately effects a cytotoxic response. We previously reported that the pyrrolo[2,3-*d*]pyrimidine antifolate **3** adopts different poses when bound to FR α versus when bound to its target enzyme GARFTase (**Figure 3**).^{27,28} As an extension of this concept, since amides assume distinct conformations as *cis* and *trans* rotamers with the lowest energy conformers,²⁹ we reason that an analog with a unique amide linkage in the bridge region would afford a

somewhat restricted three atom bridge, compared to a more flexible three carbon (CH₂) bridge. For the former, this could derive significant entropic benefit and increased target selectivity by restricting the number of side-chain conformations in both unbound and bound states. Thus, analogs that do not need to significantly alter their conformations to adopt the bound conformation at their cellular target would likely bind more effectively to target proteins than analogs that exhibit different low energy conformations



amide in the chain



compared to their bound conformations.³⁰

Figure 3. Compound **3** and its two different poses in FR α and GARFTase, as well as newly designed compounds **7-12**.

To test this concept and to begin developing new targeted inhibitors as selective cytotoxic agents for cancer, we designed a novel series of amide-bridge 6-substituted pyrrolo[2,3-*d*]pyrimidine antifolates with different energy barriers between the *cis* and *trans* conformers. It was of interest to determine the effect of inserting an amide in the bridge region on biological activity and transport selectivity for FR α and/or PCFT over RFC for three C-atom-bridge compounds such as **1**. In this report, we describe the synthesis and biological activities of the unique amide-substituted pyrrolo[2,3-*d*]pyrimidine compounds **7-12** (**Figure 3**). In designing this series, we also introduced an *N*-methyl group on the amide nitrogen to augment the metabolic stability of the amide linkage from possible enzymatic hydrolysis to make these more generally useful.³¹ Our results establish these compounds as potent and highly selective FR-targeted inhibitors of *de novo* purine biosynthesis at GARFTase, and likely at 5-aminoimidazole-4-carboxamide (AICA) ribonucleotide formyltransferase (AICARFTase) (**Figure 3**).

2. RESULTS AND DISCUSSION

2.1. Rationale for compound design

It was of interest to determine if introducing an amide into the 3-atom bridge of 6-substituted pyrrolo[2,3-*d*]pyrimidine compounds (**7-12**) would decrease the number of low energy accessible conformations, compared to the corresponding 3-atom carbon chain analogs (**1**, **3-5**). By molecular modeling in Maestro,³² we determined that the amide bridge analogs afforded a reduced number of conformations compared to their corresponding 3-carbon atom bridge analogs (**Table 1**). This suggests that amide group insertion into the side-chain as in **7-12** should provide a distinct entropic advantage that should favor binding to cellular targets.

Table 1. Conformational search results using Maestro 11.8. Target compounds (blue) and lead compounds (black)

Compound (Ar)	Number of conformations within 5 kcal/mol of minimum energy conformation
1 (1,4-phenyl)	219
7 (1,4-phenyl)	143 ↓
8 (1,3-phenyl)	152 ↓
12 (1,4-phenyl)	121 ↓
3 (2,5-thienyl)	192
9 (2,5-thienyl)	134 ↓
4 (2,4-thienyl)	148
10 (2,4-thienyl)	97 ↓
5 (3,5-thienyl)	131
11 (3,5-thienyl)	83 ↓

From our previous studies, the side-chain aromatic ring is an important determinant of drug potency and transport selectivity of 6-substituted pyrrolo[2,3-*d*]pyrimidine inhibitors.^{25,33,34} Thus, different regioisomers involving a side-chain phenyl ring and its replacement with thienyl regioisomers profoundly impacted (generally improved) compound potency. Accordingly, we designed amide-bridge analogs, with side-chain 1,4- and 1,3-disubstituted phenyl (**7** and **8**), and 2,5-, 2,4- and 3,5-di-substituted thienyl moieties (**9-11**) (**Figure 3**), based on the parent molecules (**1**, **3-5**), in order to determine the optimal side-chains for selective cellular uptake by FR α vis á vis RFC and for inhibition of intracellular target enzymes (i.e. GARFTase) resulting in antitumor activity. Finally, we designed a sulfonamide bridge compound **12** (**Figure 3**) as a bioisosteric replacement of the amide in **7**.³²

To determine the rotational barrier around the amide (N(CH₃)-C(O)) bond, we performed a coordinate scan³⁵ of target compounds **7-12** around the bridge amide bond, and of the parent compounds (**1**, **3-5**) around the C-C bond (Maestro 11.8). The resulting plot of relative energy (ΔE , kcal/mol) versus the dihedral angle (°) is shown in **Figure 4**. For the amide compounds (**7-12**), a coordinate scan predicted two distinct minimum energy conformations with *trans* and *cis* conformations of the amide bond and a high

energy barrier (~8-20 kcal/mol) between them. In contrast, a torsional scan of the carbon bridge analogs (**1**, **3-5**) predicted three distinct minimum energy conformations with a low energy barrier among them (~5 kcal/mol). This demonstrates the conformational restriction associated with the amide bridge. Based on these results, we propose that reducing the number of low energy conformations (**Table 1**) and increasing the energy barrier between bridge amide rotamers (**Figure 4**) in the target compounds (**7-12**) could enhance drug activity, reflecting uptake via FR α and inhibition of intracellular enzymes such as GARFTase.

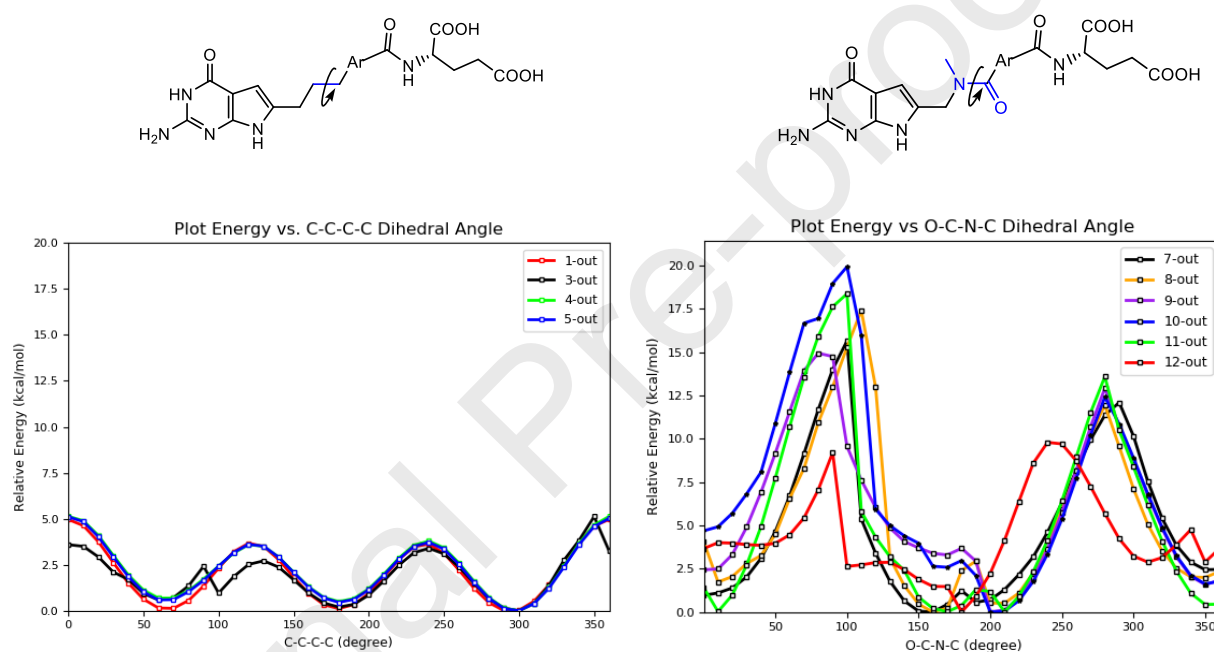


Figure 4. Plots of rotational barrier (relative energy, kcal/mol) around the carbon-carbon bridge of compounds **1**, **3**, **4** and **5** (left) and the bridged amide bond of compounds **7-12** (right). Coordinate Scan panel of Maestro 11.8 was used to determine and plot the rotational energy barrier for both the amide bridge and lead compounds; the settings were as follows: Force Field, OPLS3e; Solvent, water; Coordinate to Scan, dihedral angles of amide bridge for target compounds and carbon bridge for lead compounds (the rest of the settings were kept at default).³²

We docked the amide-bridge compounds (**Figure 3**) in the FR α (PDB: 5IZQ²⁷) and GARFTase (PDB: 4ZZ1³⁴) crystal structures. **Figures 5** and **6** show the docked poses of compound **7** in FR α and GARFTase, respectively. The amide bridge in **7** adopts both *cis* and *trans* conformations within 1 kcal/mol (docking score) for both the FR α and GARFTase structures. The major binding interactions of **7** with the target proteins are similar to those for the co-crystallized ligands **6** (FR α)²⁷ and **5** (GARFTase)³⁴. The

oxygen atom of the bridge amide group of **7** in both rotamers can form an ion-dipole interaction (distance: 2.78 Å and 2.67 Å, **Figure 6**) with the terminal amino group of the substrate GAR in the GARFTase binding site. Compound **7** shows better docking scores (FR α = -14.77 kcal/mol and GARFTase = -15.23 kcal/mol) than compound **1** (FR α = -13.33 kcal/mol and GARFTase = -14.43 kcal/mol), suggesting its more avid binding to these target proteins and predicting greater potency. The docked poses of **8** (FR α = -14.27 kcal/mol and GARFTase = -14.72 kcal/mol) and **9** (FR α = -15.23 kcal/mol and GARFTase = -14.75 kcal/mol) mimic those for **7** in FR α and GARFTase.

Compounds **10** (side-chain 2,4-thienyl) and **11** (side-chain 3,5-thienyl) were designed to vary the distance between the amide bridge and the glutamyl side-chain, and hence their conformations in comparison to the 2,5-thienyl side-chain analog **9**.³⁴ These changes introduce additional conformational restrictions and further reduce the number of possible low energy conformations even further (to 97 for **10** and 83 for **11**, compared to the 134 possible conformations for the 2,5-thienyl side-chain analog **9**; **Table 1**). Compound **12** is designed to explore the bioisosteric replacement of the amide group in compound **7**. The sulfonamide moiety in compound **12** further reduces the number of possible low energy conformations compared to **7** (**Table 1**). Compounds **10** (FR α = -12.71 kcal/mol and GARFTase = -13.31 kcal/mol), **11** (FR α = -12.75 kcal/mol and GARFTase = -12.87 kcal/mol) and **12** (FR α = -13.42 kcal/mol and GARFTase = -13.53 kcal/mol) show comparable docking scores to compounds **1** (FR α = -13.33 kcal/mol and GARFTase = -14.43 kcal/mol) and **3** (FR α = -13.67 kcal/mol and GARFTase = -14.12 kcal/mol) for both FR α and GARFTase. Moderate docking scores of the compounds **10**, **11** and **12** suggest that despite the conformational restriction, the nature of the aromatic side-chain and the bridge linker may dictate the binding affinity for the proposed compounds.

Based on our *in silico* studies, we predicted that compounds **7-12** with the amide group in the bridge should exhibit significant cellular uptake by FR α , resulting in GARFTase inhibition and antitumor efficacy. On the basis of the better docking scores in FR α and GARFTase, **7**, **8** and **9** are predicted to be more potent inhibitors of tumor growth compared to **10-12** and the lead compounds **1-6**.

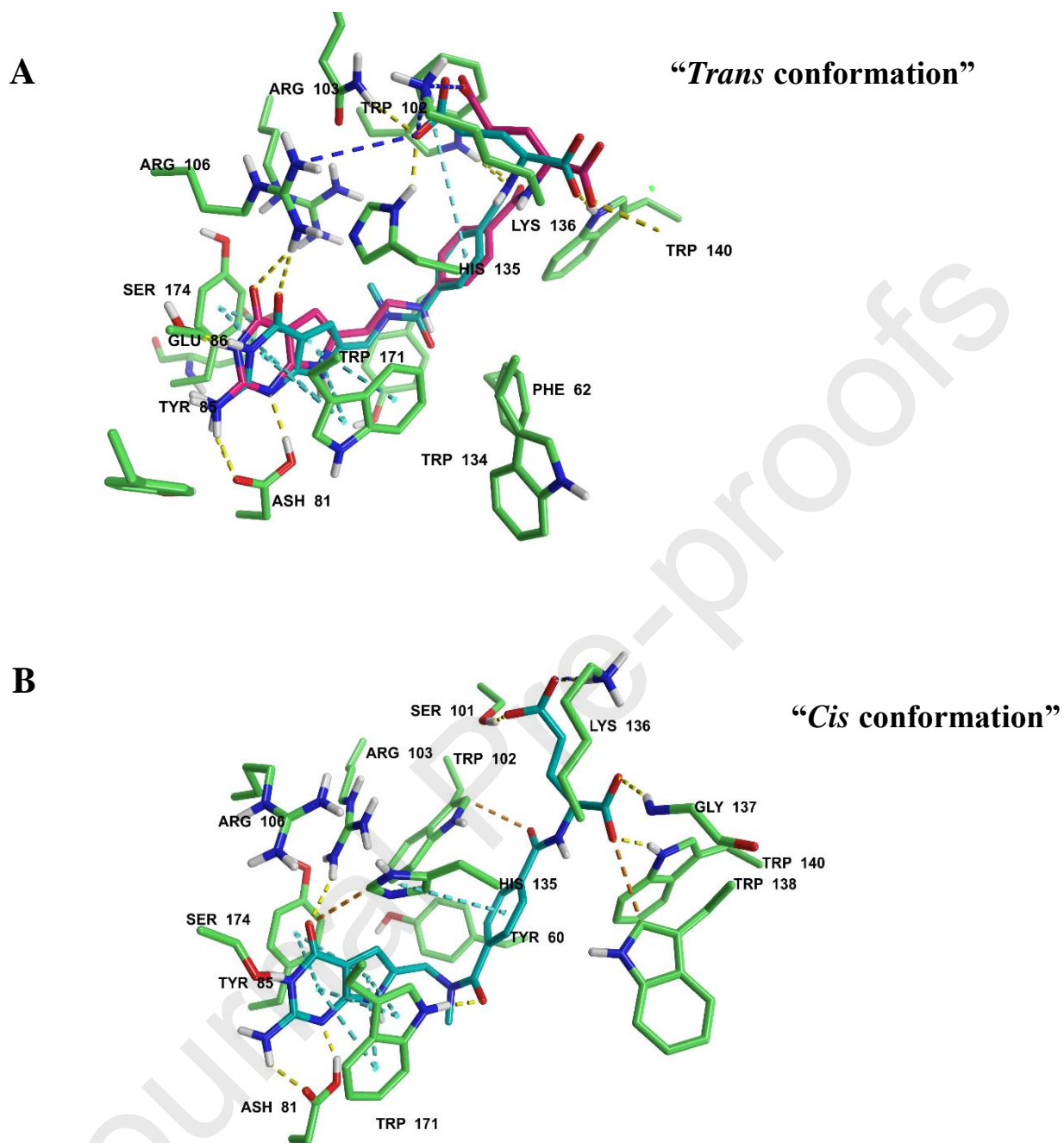


Figure 5. Two alternate docked poses of **7** in FR α (PDB ID: 5IZQ). **A**) Cyan: compound **7**, and pink: **6** (co-crystallized ligand). The amide linker in **7** adopted a *trans* conformation. Docking score: -14.77 kcal/mol. **B**) The amide linker in **7** adopted a *cis* conformation. Docking score: -13.89 kcal/mol. Maestro 11.8.

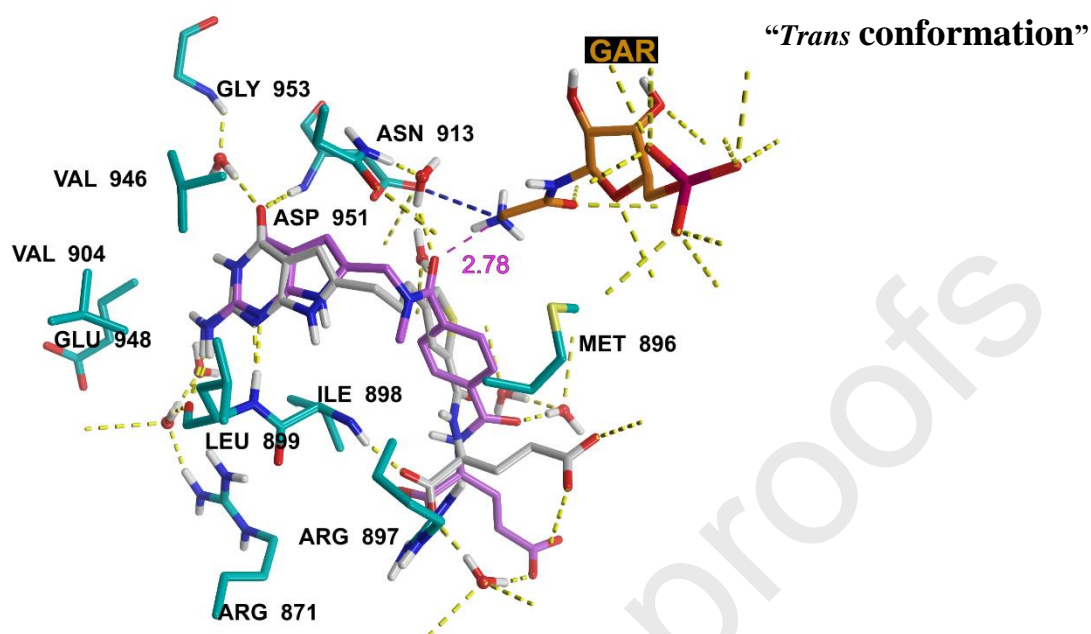
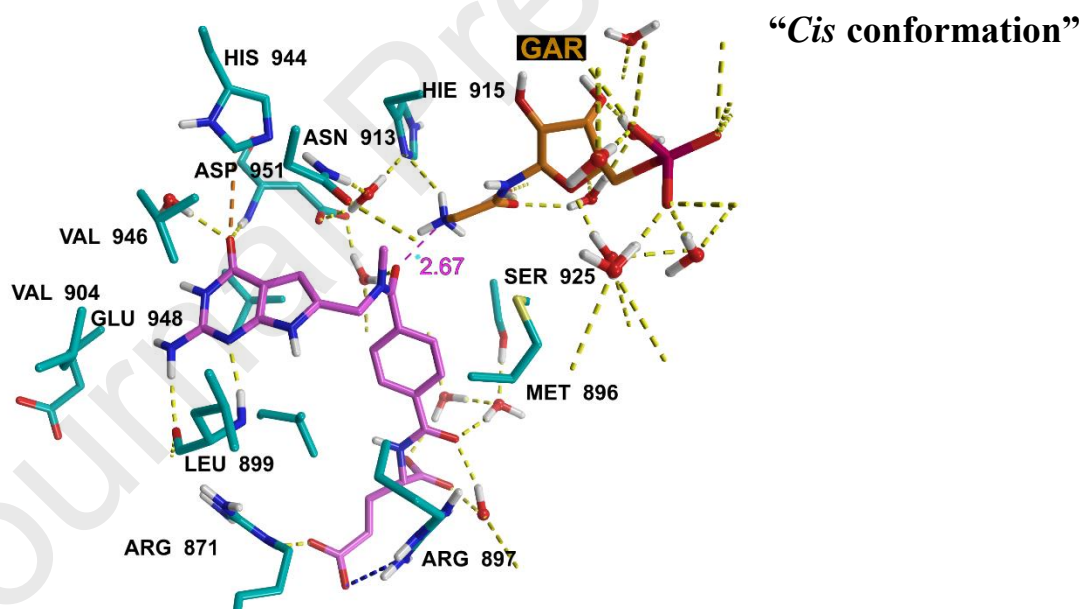
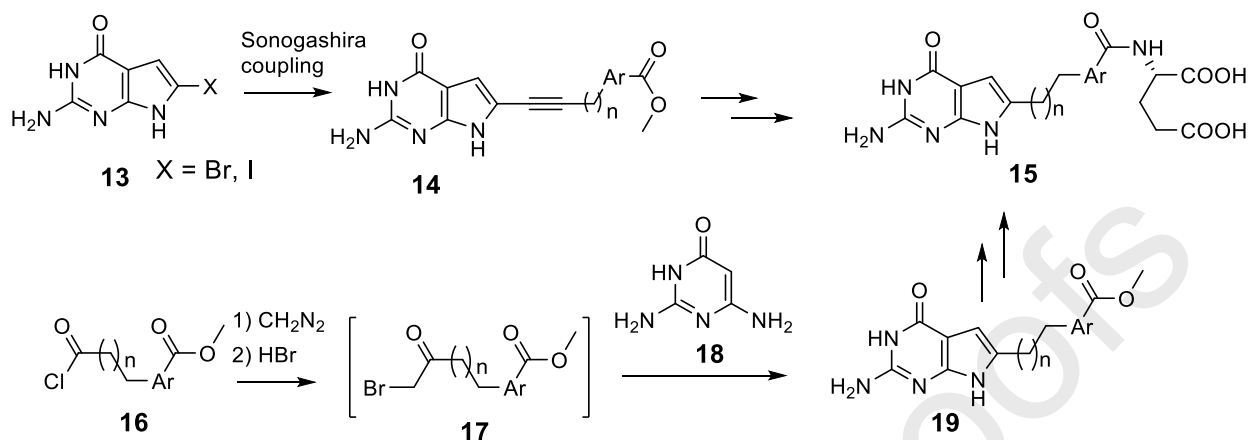
A**B**

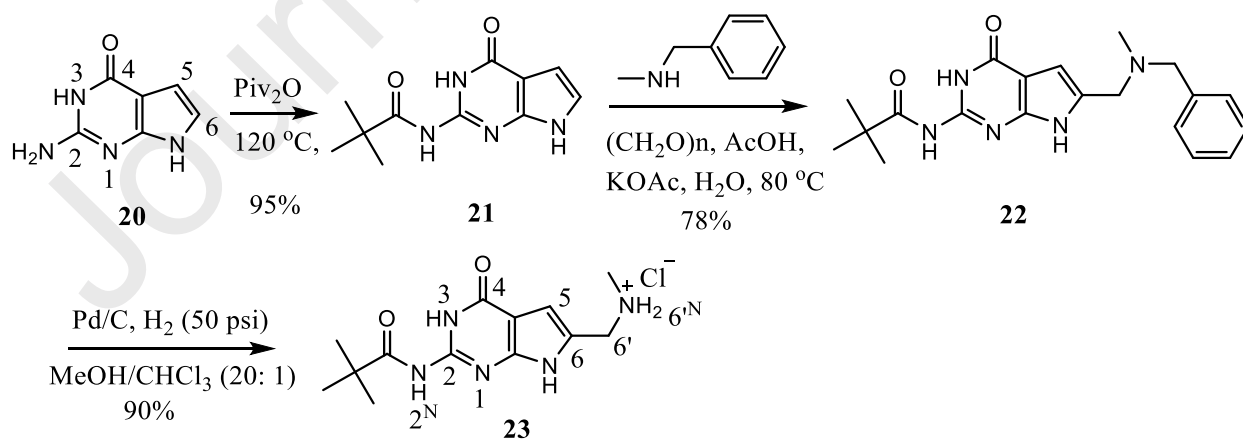
Figure 6. Two alternate docked poses of **7** in GARFTase (PDB ID: 4ZZ1). **A)** Purple, compound **7**, gray **5** (co-crystallized ligand), and red, **GAR** (endogenous substrate). The amide linker in **7** adopted a *trans* conformation. Docking score: -15.23 kcal/mol. **B)** Purple, compound **7**. The amide linker in **7** adopted a *cis* conformation. Docking score: -14.79 kcal/mol. Maestro 11.8.

3. Chemistry



Scheme 1. Two current synthesis methods for antifolate **15**.

There are two synthetic methods available for 6-substituted classical antifolates **15** (**Scheme 1**).^{34,36} The first method uses a Sonogashira coupling to install an alkyne linker on 6-halogenated pyrrolo[2,3-*d*]pyrimidines **13** and provides key intermediates **14**. This approach is not suitable for heteroatom side chain compounds.³⁶ The second method is to cyclize an α -bromoketone **17** with 2,6-diamino-4-hydroxy pyrimidine **18**, which affords the pteric ester precursors **19**. In this approach, diazomethane is an indispensable, yet dangerous, starting material.³⁷ Hence, a third synthetic method was devised for our proposed amide compounds to avoid the diazomethane reaction.



Scheme 2. Synthesis of *N*-monosubstituted 6-amiomethyl pyrrolo[2,3-*d*]pyrimidines **23**.

Our synthesis for the 6-aminomethyl pyrrolo[2,3-*d*]pyrimidines is shown in **Scheme 2**. Pivaloylation of the 2-amino moiety of the pyrrolo[2,3-*d*]pyrimidine **20** provided **21** (95% yield). The purpose of this step was to decrease the polarity and increase the solubility of **20**. The product **21** was directly precipitated from the reaction mixture by adding a mixture of hexane and ethyl acetate (5:1). Subsequently, a Mannich reaction with **21** afforded **22** in 78% yield. Finally, Pd-catalyzed debenzylation of **22** provided **23** in 90% yield.

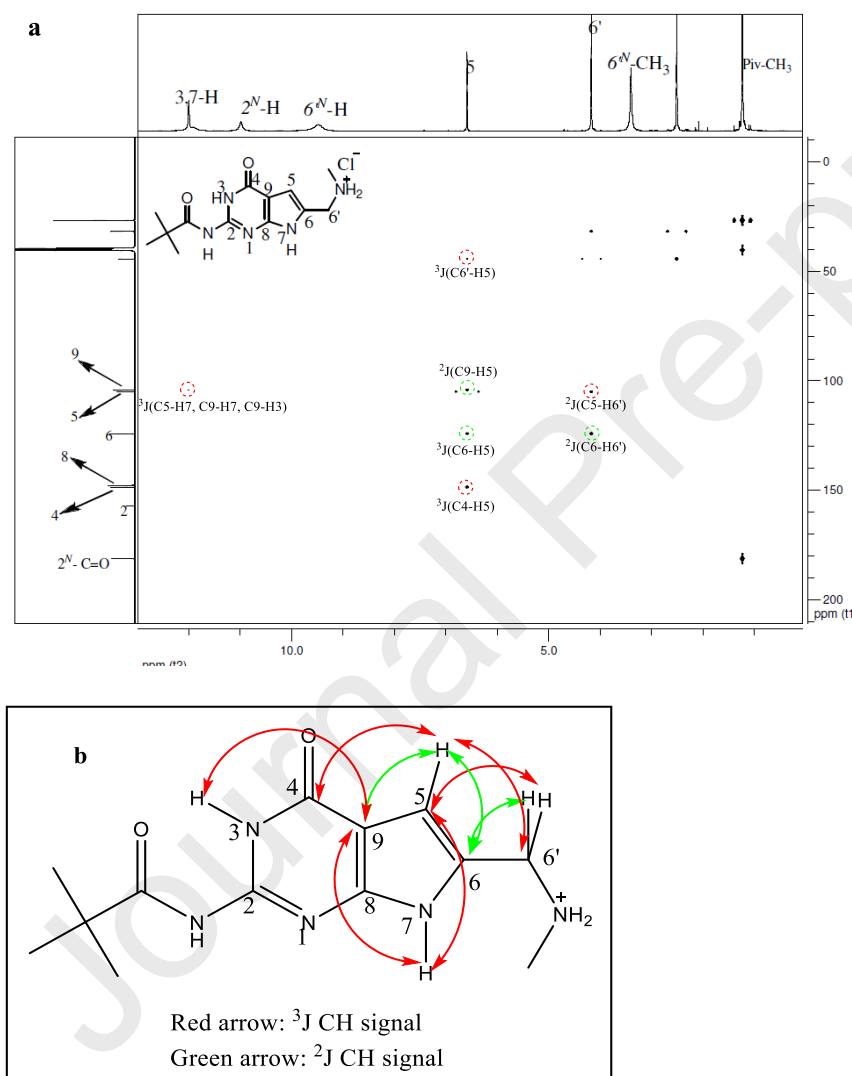
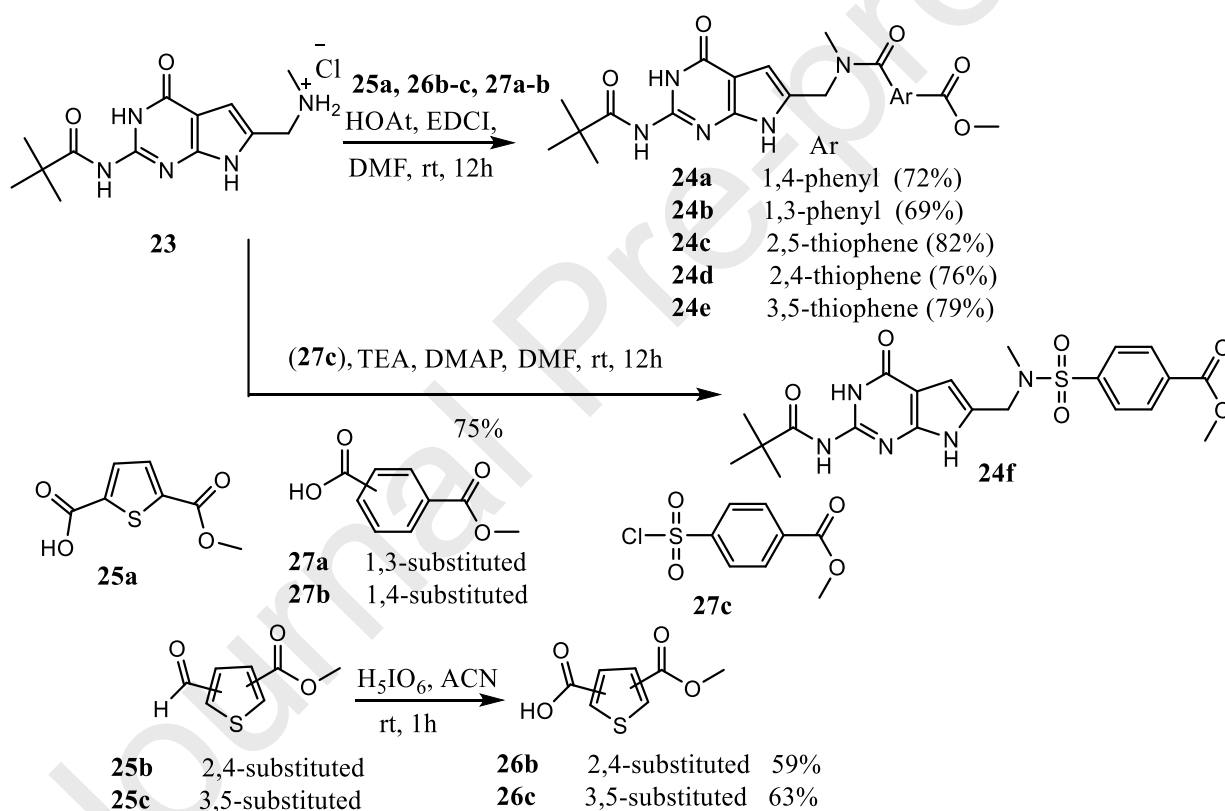


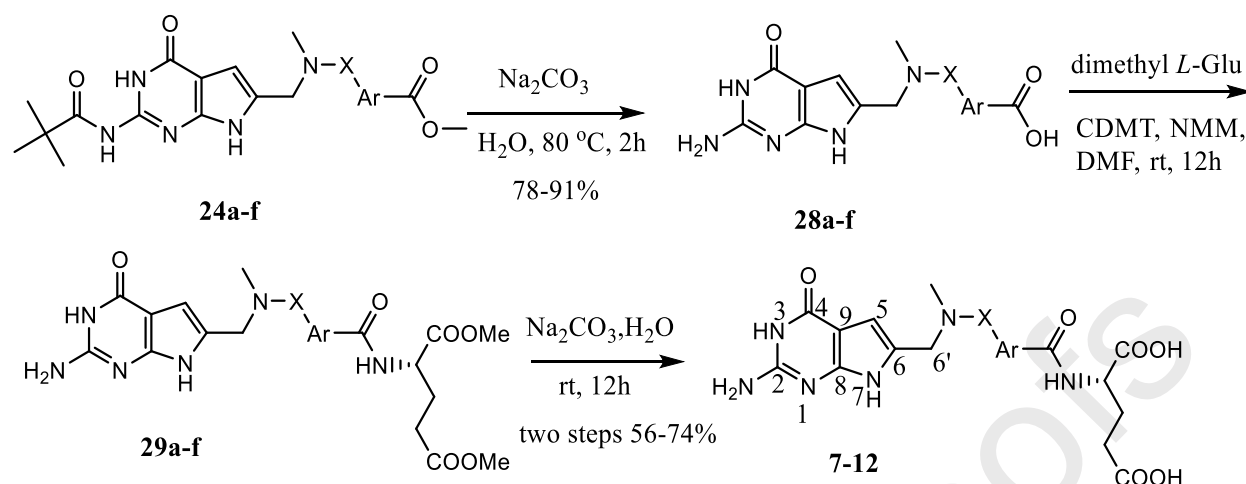
Figure 7. HMBC spectrum of **23**. a) HMBC spectrum and interpretation. The diagnostic 3J CH couplings are circled in red, and 2J CH couplings are circled in green; b) Highlighted diagnostic HMBC signals. 3J CH signals are highlighted with red arrows and 2J CH signals are highlighted with green arrows.

Since the Mannich reaction³⁸⁻⁴¹ could afford 5- and/or 6- position substituted regioisomers of the pyrrolo[2,3-*d*]pyrimidine, we analyzed the regioselectivity of the reaction from **21** to **22** with compound **23** using NOESY⁴² and HMBC (**Figure 7**). A weak NOE signal of *N*7-H and 6'-H was observed. The weak NOE signal is explained by the quadrupole *N*7-H. In HMBC (**Figure 7**), the signal of ³J(C4-H5), as well as ³J(C5-H7 and C9-H3), confirmed the structure as **23** with the aminomethyl substitution at the 6-position. This demonstrated that under our Mannich reaction conditions, the 6-substituted regioisomer was the predominant product. In addition, our synthesis provided a secondary amine in **23**, which was amenable to functionalization.



Scheme 3. Synthesis of **24a-f**.

Amide or sulfonamide coupling of **23** (**Scheme 3**) with the corresponding acid **25a**, **26b-c**, **27a-b** or methyl 4-(chlorosulfonyl)benzoate **27c** afforded **24a-f** in 69-82% yield. Compounds **26b-c** were, in turn, synthesized by periodic acid oxidation of the corresponding aldehydes **25b-c** in 56-63% yields.



Scheme 4. Synthesis of target compounds **7-12**.

Depivaloylation and hydrolysis of the methyl esters in **24a-f** (**Scheme 4**) with sodium carbonate afforded pterioic acids **28a-f** in 78-91% yields. CDMT auxiliary amide coupling of **28a-f** with dimethyl L-glutamate afforded **29a-f**. Sodium carbonate hydrolysis of **29a-f** provided the target classical antifolates **7-12** in 56-74% yields over two steps.

The ^1H NMR of **7** (**Figure 8**) exhibited two sets of peaks of the NCH_3 , NCH_2 and 5-H, for a mixture of the *cis* and *trans* rotamers, with all other protons at the same chemical shift. In each rotamer, the NCH_3 , NCH_2 and 5-H have an integration ratio of 3 to 2 to 1, which was used to assign peaks to the two different sets. The chemical shifts of protons for the *cis* conformation of the amide oxo moiety are larger than those of the *trans* conformation.⁴³ As a result, the red set (**Figure 8**) are assigned to the *cis* while the blue set are the peaks for the *trans*. This NMR result corroborates the two lowest energy rotamers of **7**, as predicted by molecular modeling.

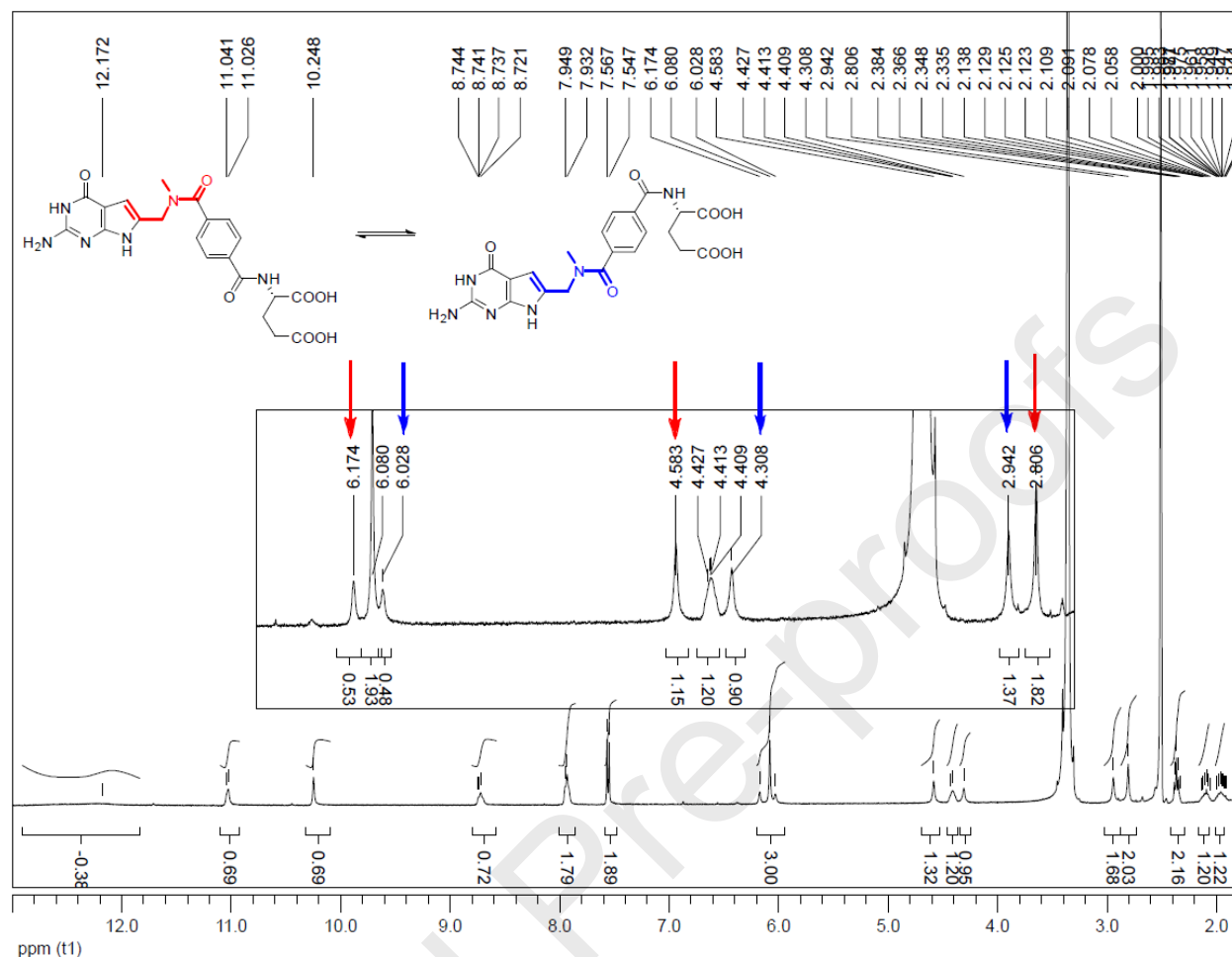


Figure 8. ^1H NMR (DMSO- d_6) of **7** at 400 MHz, the proton of NCH_3 , NCH_2 and 5-H in the *cis* and *trans* rotamers are illustrated as red and blue, respectively. Red: δ 2.81 (1.82H, *cis* NCH_3), 4.58 (1.15H, *cis* NCH_2), 6.17 (0.53H, *cis* 5-H); Blue: δ 2.94 (1.3H, *trans* NCH_3), 4.58 (0.9H, *trans* NCH_2), 6.17 (0.48H, *trans* 5-H).

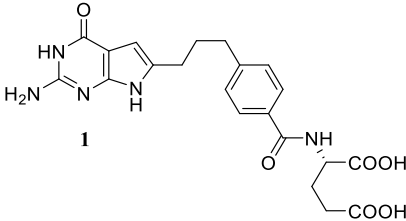
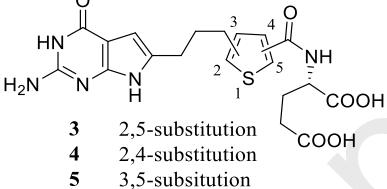
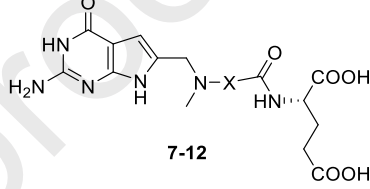
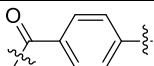
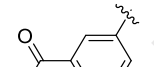

4. Biological evaluation

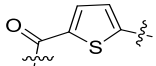
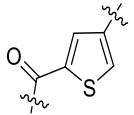
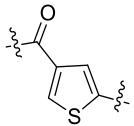
The bridge amide-substituted pyrrolo[2,3-*d*]pyrimidine compounds **7–12** were initially tested in cell proliferation assays with a unique panel of isogenic Chinese hamster ovary (CHO) cell lines engineered to individually express human RFC (PC43-10), PCFT (R2/PCFT4), or FR α (RT16).^{23,24,44} The results with the amide series were compared to previous 6-substituted pyrrolo[2,3-*d*]pyrimidine analogs with an alkyl bridge linked to side-chain phenyl (**1**)²³ or thienyl (**3–5**)^{25,34} rings, as appropriate, and to standard antifolates

(e.g., MTX) without transporter selectivity. The negative control for these experiments was the RFC-, FR-, and PCFT-null MTXR^{II}Oua^R2-4 (R2) CHO cell line.⁴⁵ For the FR α -expressing CHO cells, additional control involved treatment with excess folic acid (200 nM) to selectively block cellular uptake by FR (not shown). Proliferation experiments were also performed with KB human tumor cells that express highly elevated FR α , along with RFC and PCFT. These results are summarized in **Table 2**.

As previously reported, the non-amide pyrrolo[2,3-*d*]pyrimidine compounds (**1**, **3-5**) were potent inhibitors of CHO cells expressing FR α or PCFT and are some of the most active analogs identified for this structural platform;^{4,23,25,34} however, this activity was not selective for FR α and/or PCFT as these compounds were taken up by a non-specific (i.e., non-mediated) process that results in equivalent growth inhibition toward RFC-expressing (PC43-10) and transporter-null (R2) cells^{23,25,34} (**Table 2**). Notably, the amide-substituted compounds, **7**, **8** and **9** were inert toward RFC-expressing PC43-10 cells. Compounds **7**, **8** and **9** all preserved FR α activities, reflected in growth inhibition of RT16 and KB tumor cells (**Table 2**). Thus, compounds **7**, **8** and **9** were completely selective for FR α over RFC. For **7**, inhibition of RT16 cells (FR α) significantly exceeded (~3-fold) that for the corresponding parent analog (**1**) ($p < 0.05$), consistent with the notion that the presence of the amide bridge favors a conformation optimal for FR binding and internalization. While regioisomer **8** (*meta* substitution on the side chain phenyl ring) was equally potent as **7** toward FR α -expressing RT16 cells, **8** (*meta*-substituted on the side-chain phenyl) was ~4-fold less active than **7** (*para* substituted on the side chain phenyl ring) toward KB tumor cells (**Table 2**). Although these results may reflect factors unrelated to FR α internalization, it nonetheless suggests that that decreased distance between the scaffold and the L-glutamate moiety as in **8** compared to **7** is detrimental to antitumor activity, as previously described.²⁷ Isosteric replacement of the phenyl side chain in **7** with a thiophene ring resulted in modestly decreased growth inhibition (for **9**), or a substantial reduction (**11**) or complete loss (**10**) of FR α -targeted inhibition of RT16 and/or KB cells. The sulfonamide analog **12** was inactive regardless of the expressed transporter (**Table 2**).

Table 2. Structures of **1-12** and the IC₅₀ values for inhibition of proliferation of transporter null (R2), FR α (RT16), PCFT (R2/PCFT4), and RFC (PC43-10)-expressing CHO cells, and KB human tumor cells (expresses FR α , RFC, and PCFT) in culture. Results are expressed as mean values (\pm standard errors) from 3-10 experiments. Abbreviations: MTX, methotrexate; PMX, pemetrexed; RTX, raltitrexed. *These data were previously published (see reference).

<div style="display: flex; justify-content: space-around; align-items: center;"> <div style="text-align: center;">  <p>1</p> </div> <div style="text-align: center;">  <p>3 2,5-substitution 4 2,4-substitution 5 3,5-substitution</p> </div> <div style="text-align: center;">  <p>7-12</p> </div> </div>							
Compound	X	IC ₅₀ (nM)					Reference
		PC43-10 (RFC)	R2	RT16 (FR α)	R2/PCFT4 (PCFT)	KB (FR α /RFC/PCFT)	
1*	-	304 (89)	448 (78)	4.1(1.6)	23.0(3.3)	1.7(0.4)	46
7		>1000	>1000	1.4(0.24)	48.60(16.40)	1.40(0.24)	-
8		>1000	>1000	1.78 (0.17)	747 (156)	6.36 (1.00)	-
12		>1000	>1000	>1000	>1000	669 (112)	-

3	-	101.0 (16.6)	273.0(49.1)	0.31 (0.14)	3.34 (0.26)	0.26 (0.03)	25
9		>1000	>1000	7.78(1.63)	>1000	4.23(0.57)	-
4*	-	189(51)	290((8)	0.61(0.11)	6.51(1.30)	0.09(0.02)	34
10		>1000	>1000	>1000	>1000	>1000	-
5*	-	197(49)	355(10)	0.33(0.15)	5.39(1.27)	0.17(0.05)	34
11		>1000	>1000	867(147)	>1000	69.8(16.1)	-
MTX*	-	12(1.1)	216(8.7)	114(31)	121(17)	6.0(0.6)	-
PMX*	-	138(13)	894(93)	42(9)	13.292.4)	68(12)	-
RTX*	-	6.3(1.3)	>1000	15(5)	99.5(11.4)	5.9(2.2)	-

While compounds **7-12** were all designed to inhibit GARFTase in *de novo* purine biosynthesis following internalization by FR α , this was directly tested for the compounds **7** and **9** with side-chain phenyl and 2,5-thiophene moieties analogous to parent compounds **1** and **3**. For these experiments, we determined the extent of growth inhibition of KB tumor cells by these compounds in the presence of thymidine (10 μ M) or adenosine (60 μ M).^{25,27,33,34,36} We also tested the protective effects of glycine (130 μ M) to explore the potential inhibition of mitochondrial C1 metabolism.⁴⁷ Results for the nucleoside/glycine protection experiments are shown in **Figure 9A**. Adenosine completely reversed the drug effects of all the compounds, whereas thymidine and glycine were completely ineffective. Thus, neither thymidylate synthase nor mitochondrial C1 metabolism are involved in the mechanism of action of **7** or **9**. The metabolite AICA (320 μ M) is metabolized to AICA ribonucleotide (ZMP), the AICARFTase substrate which circumvents the GARFTase step.^{27,28,33,34,36,44} AICA completely reversed the inhibitory effects of compounds **1** and **3** up to 1 μ M; however, at higher concentrations of **3**, AICA was less protective. By analogy with published results for related compounds,^{27,28,33,34,36,44,46} our results suggest that GARFTase is the primary intracellular target for this series, although at higher inhibitor concentrations, targeting of AICARFTase also contributes.

To further confirm GARFTase as the principal cellular target for our most potent analogs (compounds **7** and **9**), GARFTase was directly assayed *in situ* in KB cells. For these experiments, KB cells were incubated with a range of concentrations of compounds **7** or **9**, or of compounds **1** and **3** as controls, under conditions closely approximating those for the cell proliferation assays (**Table 1**). Cells were incubated with [14 C]glycine, which is incorporated into [14 C]GAR and [14 C]FGAR (the GARFTase product). The latter accumulates in the presence of azaserine (inhibits FGAR amidotransferase) and is isolated by anion exchange fractionation for quantitation and calculation of IC₅₀ values for GARFTase inhibition. All compounds inhibited GARFTase with IC₅₀ values approximately one-order of magnitude higher than that for inhibition of KB proliferation. Collectively, these results establish that *de novo* purine biosynthesis is the principal targeted pathway by the active amide-substituted pyrrolo[2,3-*d*]pyrimidine compounds **7** and **9** at GARFTase, and likely AICARFTase, as well.

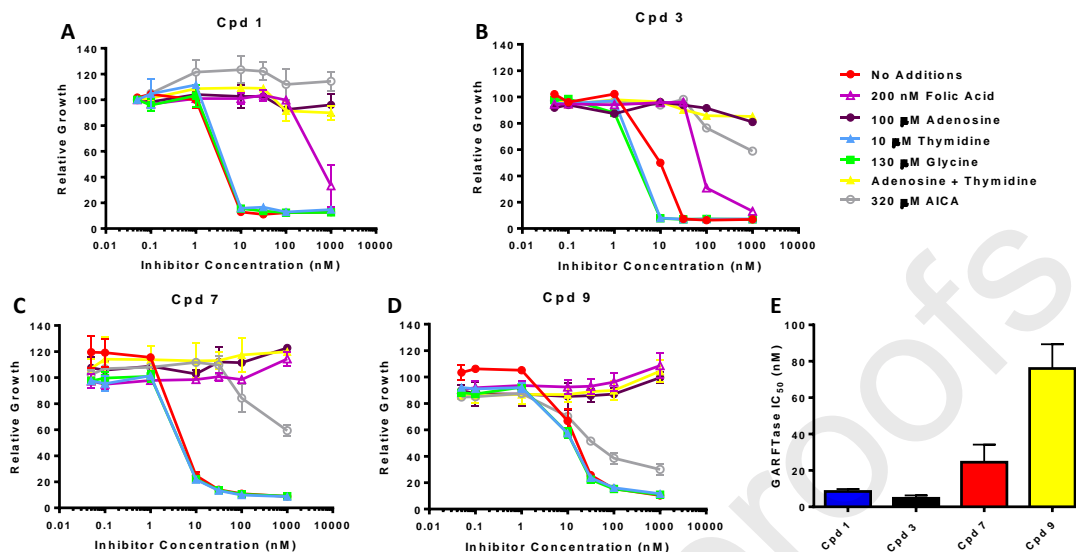


Figure 9. Identification of the intracellular target by protection by nucleosides, glycine and AICA, and *in situ* GARFTase assays. **A-D)** KB cells were incubated with drugs in folate-, nucleoside-, and glycine-free RPMI 1640 medium with 10% dialyzed FBS, antibiotics, L-glutamine, and 2 nM leucovorin with a range of drug concentrations in the presence of folic acid (200 nM), adenosine (60 μM), thymidine (10 μM), glycine (130 μM) or AICA (320 μM). Cell proliferation was assayed with Cell Titer Blue (Promega) using a fluorescence plate reader. Data are representative of at least triplicate experiments. Error bars represent the standard errors. **E)** Inhibition of GARFTase activity in KB cells by the 6-substituted pyrrolo[2,3-*d*]pyrimidine compounds including compounds **1**, **3**, **7** and **9**. KB cells were treated with the drugs under conditions approximating those for the cell outgrowth experiments (**Table 2**). Incorporation of [¹⁴C(U)]glycine into [¹⁴C]formyl GAR was used as an *in situ* measure of endogenous GARFTase activity. Experimental details are summarized in the Experimental Section. IC₅₀ values (nM) were calculated as mean values +/- standard errors for triplicate experiments.

5. Conclusion

In this study, we used molecular modeling and docking studies to rationally design a series of amide-bridged pyrrolo[2,3-*d*]pyrimidine antifolates with *cis* and *trans* conformations as the two lowest energy conformations. These conformations were supported by ¹H NMR analysis. We previously described carbon-bridge analogs of this series (**1** - **6**) that are not selective for FR and PCFT over other uptake mechanisms including RFC^{23,25,36} that allows the accumulation of the analogs in normal tissues and precludes tumor selectivity. Based on proliferation studies in isogenic CHO cell lines exclusively expressing human FRα, PCFT or RFC, we determined that the active amide compounds **7-9** are transported

by FR α with or without PCFT, but not by RFC, and thus should possess absolute tumor selectivity. This indicates that the amide bridge is highly conducive to tumor transport selectivity for **7-9**. Based on the inhibitory results toward KB human tumor cells, compounds **7** and **9** were tested to identify the likely targeted pathway and enzyme(s) in comparison to compounds **1** and **3**, previously identified as exclusive inhibitors of GARFTase in *de novo* purine nucleotide biosynthesis.^{23,25} Whereas compounds **7** and **9** were confirmed as GARFTase inhibitors by nucleoside/AICA protection, a secondary target, most likely AICARFTase, was also implicated.

Our original hypothesis was that conformational restriction caused by the amide bridge in the analogs **7-12** would favor targeting FR α and possibly GARFTase by our analogs. Consistent with our hypothesis, compound **7** was ~3-fold more potent than **1** toward CHO cells exclusively expressing FR α , although **7** and **1** are equipotent toward KB cells that express RFC, FR α and PCFT. This suggests that the conformational restriction in **7** promotes FR α -targeting of our analogs, although at least for this analog, uptake by PCFT is preserved, as well, likely contributing to drug effects in KB cells. In the absence of crystal structures for RFC and PCFT, the information from this study can guide the design of conformationally restricted compounds that are exclusively transported by FR α -expressing cancer cells to afford highly selective, non-toxic cancer chemotherapeutic agents.

6. Experimental Section

Analytical samples were dried in vacuum (0.2 mmHg) in a CHEM-DRY drying apparatus over P₂O₅ at 50 °C. Melting points were determined on a digital MEL-TEMP II melting point apparatus with FLUKE 51K/J electronic thermometer and are uncorrected. Nuclear magnetic resonance spectra for protons (¹H NMR, ¹³C NMR and HMBC) were recorded on a Bruker Avance II 400 (400 MHz) or on a 500 (500 MHz) NMR systems. The chemical shift values are expressed in ppm (parts per million) relative to tetramethylsilane as an internal standard: s, singlet; d, doublet; t, triplet; q, quartet; quint, quintet; m, multiplet; br, broad singlet. Thin-layer chromatography (TLC) was performed on Whatman Sil G/UV254

silica gel plates with a fluorescent indicator, and the spots were visualized under 254 and 365 nm illumination. Proportions of solvents used for TLC are by volume. Column chromatography was performed on a 230–400 mesh silica gel (Fisher Scientific) column. Elemental analyses were performed by Atlantic Microlab, Inc., Norcross, GA. Elemental compositions are within $\pm 0.4\%$ of the calculated values and indicate $> 95\%$ purity of the compounds. Fractional moles of water or organic solvents found in some analytical samples could not be prevented despite 24 h of drying in vacuum and were confirmed where possible by their presence in the ^1H NMR spectra. UPLC-MS was analyzed on Acquity system. A linear gradient of 90% of 0.1% formic acid in water, 10% of 0.1% formic acid in acetonitrile (ACN) over 10 min, and then 100% ACN was used for 5 min. All final compounds were $> 95\%$ purity established by CHN, or UPLC-MS, or both CHN and UPLC-MS. All solvents and chemicals were purchased from Sigma-Aldrich Co. or Fisher Scientific Inc. and were used as received.

2-Pivalamido-4-oxo-4,7-dihydro-1H-pyrrolo[2,3-*d*]pyrimidine (21)

2-Amino-4-oxo-4,7-dihydro-1H-pyrrolo[2,3-*d*]pyrimidine (**20**) (3.0 g, 20 mmol) was added to pivalic anhydride (12 mL). The resulting suspension was stirring at 90 °C for 3 h. The reaction was cooled to rt and a mixture of hexane (40 mL) and EtOAc (8 mL) was added dropwise. The suspension was filtered, washed with acetone (10 mL), and dried at 50 °C under vacuum overnight to afford 4.44 g of pale yellow solid **21** in 95% yield. mp > 250 °C (lit⁴⁸ 295 °C); TLC *R_f* 0.55 (CHCl_3 : MeOH, 20:1); ^1H NMR ($\text{DMSO-}d_6$) δ 1.28 (s, 9H, Piv), 6.41 (d, $J = 4.2$ Hz, 1H, 5-H), 6.95 (d, $J = 4.2$ Hz, 1H, 6-H), 10.73 (br, 1H, exch, PivNH), 11.55 (br, 1H, exch, NH), 11.83 (br, 1H, exch, NH).

2-Pivalamido-4-oxo-6-(*N*-methyl-benzylaminomethyl)-4,7-dihydro-3H-pyrrolo[2,3-*d*]pyrimidine (22)

N-Methyl benzylamine (3.63 g, 30 mmol) and paraformaldehyde (1.05 g, 35 mmol) were added to water (20 mL). To this solution, acetic acid (20 mL) was added dropwise. The mixture was stirred at 80 °C for 3 h. Compound **21** (2.34 g, 10 mmol) and KOAc (2.94 g, 30 mmol) were added and the stirring was continued at 80 °C overnight. The solvent was removed by a rotary evaporator and acetone (40 mL) was added. The

suspension was filtered and the filtrate was concentrated into a semisolid residue. This residue was purified by a silica column, which was flushed with CHCl₃ and MeOH, to provide 2.86 g of a white solid, **22**, in 78% yield. mp: 181.1 - 182.5 °C; TLC *R_f* 0.37 (CHCl₃: MeOH, 20:1); ¹H NMR (DMSO-d₆) δ 1.24 (s, 9H, Piv), 2.09 (s, 3H, NCH₃), 3.48 (s, 2H, NCH₂), 3.58 (s, 2H, NCH₂), 6.31 (s, 1H, 5-H), 7.32 (m, 5H, Ph), 10.85 (br, 1H, exch, PivNH), 11.55 (br, 1H, exch, NH), 11.95 (br, 1H, exch, NH); Anal. calcd. for (C₂₀H₂₅N₅O₂·0.5H₂O) C, H, N; UPLC-MS > 95%; *m/z* [M-MePhNH]⁺, calcd 247.12, found 247.25.

2-Pivalamido-4-oxo-6-(methylaminomethyl)-4,7-dihydro-3H-pyrrolo[2,3-*d*]pyrimidine hydrochloric salt (23)

Compound **22** (1.84 g, 5 mmol) was dissolved in methanol (40 mL) and chloroform (2 mL) in a Parr hydrogenation flask. Pd/C (10%, 200 mg) was added to the above solution under Ar atmosphere and placed on the Parr hydrogenation shaker under 50 psi hydrogen for 2 h. The catalyst was filtered through celite, and the solvent was evaporated. To the residue was added acetone (5 mL) and the suspension was filtered, and dried to afford 1.41 g of **23** as a white solid in 90% yield. mp > 250 °C; TLC *R_f* 0.13 (CHCl₃: MeOH, 10:1); ¹H NMR (DMSO-d₆) δ 1.24 (s, 9H, Piv), 3.07 (s, 3H, NCH₃), 4.17 (s, 2H, NCH₂), 6.58 (s, 1H, 5-H), 9.32 (br, 2H, exch, NH₂⁺), 10.95 (br, 1H, exch, PivNH), 11.86 (br, 2H, exch, NH); ¹³C NMR (DMSO-d₆) δ 31.99, 44.48, 104.34, 105.09, 127.39, 148.67, 148.73, 157.11, 181.37; UPLC-MS > 95%; *m/z* [M-MeNH]⁺, calcd 247.12, found 247.18.

General procedures for the synthesis of methoxycarbonyl thiophene carboxylic acids 26b-c

To methoxycarbonyl thiophene carboxylaldehyde **25b-c** in acetonitrile solution, periodic acid (2 eq.) was added and the reaction was stirred at rt for 1 h. To the above solution, water (10 mL) was added and mixture was extracted with EtOAc (3 X 10 mL). The organic layers were combined, dried, concentrated, and purified by a silica column with CHCl₃ and MeOH, to provide a white solid **26b-c**.

2-Methoxycarbonyl-thiophene-4-carboxylic acid (26b)

Yield: 59%. mp 136.9 - 137.8 °C; TLC *R_f* 0.22 (CHCl₃: MeOH, 20:1); ¹H NMR (CDCl₃) δ 3.93 (s, 3H, OCH₃), 8.28 (d, *J* = 1 Hz, 1H, ArH), 8.37 (d, *J* = 1 Hz, 1H, ArH); Anal. calcd. for (C₇H₆O₄S·0.15H₂O) C, H, S.

3-Methoxycarbonyl-thiophene-5-carboxylic acid (26c)

Yield: 63%. mp 189.1 - 189.5 °C; TLC *R_f* 0.22 (CHCl₃: MeOH, 20:1); ¹H NMR (CDCl₃) δ 3.95 (s, 3H, OCH₃), 8.24 (s, 1H, ArH), 8.40 (s, 1H, ArH); Anal. calcd. for (C₇H₆O₄S) C, H, S.

Methyl 4-[[*N*-methyl-(2-pivalamido-4-oxo-4,7-dihydro-3H-pyrrolo[2,3-*d*]pyrimidin-6-yl)-methylamino]-carbonyl]-phenylcarboxylate (24a)

To a solution of 4-methoxycarbonyl phenyl carboxylic acid (180 mg, 1 mmol) in DMF (1 mL) was added *N*-methyl morpholine (310 mg, 3 mmol), EDCI (240 mg, 1.2 mmol) and HOAt (183 mg, 1.05 mmol). The mixture was stirred at rt for 1 h. Compound **23** (313 mg, 1 mmol) was added and stirring was continued overnight. The solvent was removed and the residue was purified by a silica column with CHCl₃ and MeOH to provide 316 mg of **24a** as a semi-solid in 72% yield. TLC *R_f* 0.16 (CHCl₃/MeOH, 40:1); ¹H NMR (DMSO-*d*₆) δ 1.25 (s, 9H, Piv), 2.84 (s, 1.8H, *cis* NCH₃), 2.99 (s, 1.2H, *trans* NCH₃), 3.88 (s, 3H, OCH₃), 4.44 (s, 0.8H, *trans* NCH₂), 4.70 (s, 1.2H, *cis* NCH₂), 6.24 (s, 0.4H, *trans* 5-H), 6.38 (s, 0.6H, *cis* 5-H), 7.60 (d, *J* = 6.8 Hz, 2H, Ph), 8.04 (d, *J* = 6.8 Hz, 2H, Ph), 10.79 (br, 1H, *exch*, PivNH), 11.62 (br, 1H, *exch*, NH), 11.87 (s, 1H, *exch*, NH).

Methyl 3-[[*N*-methyl-(2-pivalamido-4-oxo-4,7-dihydro-3H-pyrrolo[2,3-*d*]pyrimidin-6-yl)-methylamino]-carbonyl]-phenylcarboxylate (24b)

Compound **24b** was synthesized following the procedure of **24a** and was obtained as a semi-solid in 69% yield. TLC *R_f* 0.15 (CHCl₃/MeOH, 40:1); ¹H NMR (DMSO-*d*₆) δ 1.25 (s, 9H, Piv), 2.73 (s, 1.2H, *cis* NCH₃),

2.85 (s, 1.8H, *trans* NCH₃), 3.98 (s, 3H, OCH₃), 4.43 (s, 0.8H, *trans* NCH₂), 4.69 (s, 1.2H, *cis* NCH₂), 6.27 (s, 0.4H, *trans* 5-H), 6.39 (s, 0.6H, *cis* 5-H), 7.62 (m, 1H, Ph), 7.75 (m, 1H, Ph), 8.03 (m, 2H, Ph), 10.79 (s, 1H, *exch*, PivNH), 11.63 (s, 1H, *exch*, NH), 11.89 (s, 1H, *exch*, NH).

Methyl 5-[[N-methyl-(2-pivalamido-4-oxo-4,7-dihydro-3H-pyrrolo[2,3-*d*]pyrimidin-6-yl)-methylamino]-carbonyl]-thiophene-2-carboxylate (24c)

Compound **24c** was synthesized following the procedure of **24a** from **25a** and was obtained as a semi-solid in 82% yield. TLC *R_f* 0.16 (CHCl₃/MeOH, 40:1); ¹H NMR (DMSO-*d*₆) δ 1.24 (s, 9H, Piv), 3.05 (br, 3H, *cis* and *trans* NCH₃), 3.85 (s, 3H, OCH₃), 4.69 (s, 2H, *cis* and *trans* NCH₂), 6.35 (s, 1H, *cis* and *trans* 5-H), 7.54 (s, 1H, thiophene), 7.78 (s, 1H, thiophene), 10.80 (s, 1H, *exch*, PivNH), 11.62 (s, 1H, *exch*, NH), 11.88 (s, 1H, *exch*, NH).

Methyl 4-[[N-methyl-(2-pivalamido-4-oxo-4,7-dihydro-3H-pyrrolo[2,3-*d*]pyrimidin-6-yl)-methylamino]-carbonyl]-thiophene-2-carboxylate (24d)

Compound **24d** was synthesized following the procedure of **24a** from **26b** and was obtained as a semi-solid in 76% yield. TLC *R_f* 0.17 (CHCl₃/MeOH, 40:1); ¹H NMR (DMSO-*d*₆) δ 1.25 (s, 9H, Piv), 2.89 (s, 1.5H, *cis* NCH₃), 2.89 (s, 1.5H, *trans* NCH₃), 3.80 (s, 3H, OCH₃), 4.69 (s, 2H, *cis* and *trans* NCH₂), 6.33 (s, 1H, *cis* and *trans* 5-H), 7.78 (s, 1H, thiophene), 8.54 (s, 1H, thiophene), 10.79 (s, 1H, *exch*, PivNH), 11.64 (s, 1H, *exch*, NH), 11.89 (br, 1H, *exch*, NH).

Methyl 5-[[N-methyl-(2-Pivalamido-4-oxo-4,7-dihydro-3H-pyrrolo[2,3-*d*]pyrimidin-6-yl)-methylamino]-carbonyl]-thiophene-3-carboxylate (24e)

Compound **24e** was synthesized following the procedure of **24a** from **26c** and was obtained as a semi-solid in 79% yield. TLC *R_f* 0.16 (CHCl₃/MeOH, 40:1); ¹H NMR (DMSO-*d*₆) δ 1.25 (s, 9H, Piv), 2.98 (s, 3H, *cis* and *trans* NCH₃), 3.92 (s, 3H, OCH₃), 4.65 (br, 2H, *cis* and *trans* NCH₂), 6.37 (br, 1H, *cis* and *trans* 5-H),

7.91 (d, $J = 2.8$ Hz, 1H, thiophene), 8.34 (d, $J = 3.0$ Hz, 1H, thiophene), 10.78 (s, 1H, exch, PivNH), 11.55 (s, 1H, exch, NH), 11.86 (s, 1H, exch, NH).

Methyl 4-[[*N*-methyl-(2-pivalamido-4-oxo-4,7-dihydro-3H-pyrrolo[2,3-*d*]pyrimidin-6-yl)-methylamino]-sulfonyl]-phenylcarboxylate (24f)

To a solution of **23** (313 mg, 1 mmol) in DMF (1 mL), was added triethylamine (210 mg, 2.05 mmol), methyl 4-chlorosulfonyl benzoate **27c** (235 mg, 1 mmol) and 4-dimethylaminopyridine (10 mg). The mixture was stirred at rt for 4 h. The solvent was removed and the residue was purified by a silica column with CHCl₃ and MeOH to afford 356 mg of **24f** as a white solid in 75% yield. TLC R_f 0.13 (CHCl₃/MeOH, 40:1); ¹H NMR (DMSO-*d*₆) δ 1.25 (s, 9H, Piv), 2.61 (s, 3H, NCH₃), 3.91 (s, 3H, OCH₃), 4.21 (s, 2H, NCH₂), 6.28 (s, 1H, 5-H), 7.95 (d, $J = 8.0$ Hz, 2H, Ph), 8.18 (d, $J = 8.0$ Hz, 2H, Ph), 10.85 (s, 1H, exch, PivNH), 11.66 (s, 1H, exch, NH), 11.88 (s, 1H, exch, NH).

4-[[*N*-Methyl-(2-amino-4-oxo-4,7-dihydro-3H-pyrrolo[2,3-*d*]pyrimidin-6-yl)-methylamino]-carbonyl]-phenylcarboxylic acid (28a)

To a solution of **24a** (220 mg, 0.5 mmol) in water (10 mL) and methanol (10 mL) was added Na₂CO₃ (0.5 g). The mixture was stirred at 80 °C for 2h. The methanol was removed and the pH of the solution was adjusted to 3 with 1N HCl. The suspension was filtered and the filter cake was washed with deionized water and acetone to facilitate drying, and dried to afford 152 mg white solid **28a** in 90% yield. mp > 250 °C; TLC R_f 0.53 (CHCl₃: MeOH: AcOH, 10:1:0.5); ¹H NMR (DMSO-*d*₆) δ 2.78 (s, 1.8H, *cis* NCH₃), 2.93 (s, 1.2H, *trans* NCH₃), 4.30 (s, 0.8H, *trans* NCH₂), 4.58 (s, 1.2H, *cis* NCH₂), 6.01 (s, 0.4H, *trans* 5-H), 6.07 (s, 2H, exch, 2-NH₂), 6.16 (s, 0.6H, *cis* 5-H), 7.58 (d, $J = 6.8$ Hz, 2H, Ph), 8.01 (d, $J = 6.8$ Hz, 2H), 10.25 (s, 1H, exch), 10.33 (s, 1H, exch), 13.14 (s, 1H, exch); Anal. calcd. for (C₁₆H₁₅N₅O₄ · 1.40H₂O) C, H, N; UPLC-MS > 95%; m/z [M+H]⁺, calcd 342.11, found 342.25.

3-[[N-methyl-(2-amino-4-oxo-4,7-dihydro-3H-pyrrolo[2,3-*d*]pyrimidin-6-yl)-methylamino]-carbonyl]-phenylcarboxylic acid (28b)

Compound **28b** was synthesized in 83% yield following the procedure of **28a**. mp > 250 °C; TLC *R_f* 0.51 (CHCl₃: MeOH: AcOH, 10:1:0.5); ¹H NMR (DMSO-*d*₆) δ 2.79 (s, 1.8H, *cis* NCH₃), 2.92 (s, 1.2H, *trans* NCH₃), 4.32 (s, 0.8H, *trans* NCH₂), 4.58 (s, 1.2H, *cis* NCH₂), 6.02 (s, 0.4H, *trans* 5-H), 6.08 (s, 2H, *exch*, 2-NH₂), 6.16 (s, 0.6H, *cis* 5-H), 7.58 (m, 1H, Ph), 7.72 (m, 1H, Ph), 8.18 (m, 2H, Ph), 10.26 (s, 1H, *exch*, NH), 11.06 (s, 1H, *exch*, NH), 13.20 (s, 1H, *exch*, COOH); Anal. calcd. for (C₁₆H₁₅N₅O₄ · 0.4Acetone·1.8H₂O) C, H, N; UPLC-MS > 95%; m/z [M+H]⁺, calcd 342.11, found 342.28.

5-[[N-methyl-(2-amino-4-oxo-4,7-dihydro-3H-pyrrolo[2,3-*d*]pyrimidin-6-yl)-methylamino]-carbonyl]-thiophene-2-carboxylic acid (28c)

Compound **28c** was synthesized in 82% yield following the procedure of **28a**. mp > 250 °C; TLC *R_f* 0.47 (CHCl₃: MeOH: AcOH, 10:1:0.5); ¹H NMR (DMSO-*d*₆) δ 2.95 (br, 3H, *cis* and *trans* NCH₃), 4.58 (s, 2H, *cis* and *trans* NCH₂), 6.07 (s, 2H, *exch*, 2-NH₂), 6.12 (s, 1H, *cis* and *trans* 5-H), 7.52 (s, 1H, thiophene), 7.67 (s, 1H, thiophene), 10.34 (s, 1H, *exch*, NH), 11.08 (s, 1H, *exch*, NH), 13.20 (s, 1H, *exch*, COOH); Anal. calcd. for (C₁₄H₁₃N₅O₄S · 0.1Acetone·0.95H₂O) C, H, N, S; UPLC-MS > 95%; m/z [M+H]⁺, calcd 348.07, found 348.20.

4-[[N-methyl-(2-amino-4-oxo-4,7-dihydro-3H-pyrrolo[2,3-*d*]pyrimidin-6-yl)-methylamino]-carbonyl]-thiophene-2-carboxylic acid (28d)

Compound **28d** was synthesized in 90% yield following the procedure of **28a**. mp > 250 °C; TLC *R_f* 0.50 (CHCl₃: MeOH: AcOH, 10:1:0.5); ¹H NMR (DMSO-*d*₆) δ 3.12 (br, 3H, *cis* and *trans* NCH₃), 4.59 (s, 2H, *cis* and *trans* NCH₂), 6.12 (br, 3H, 2-NH₂(*exch*), *cis* and *trans* 5-H), 7.71 (s, 1H, thiophene), 8.43 (s, 1H, thiophene), 10.28 (s, 1H, *exch*, NH), 11.10 (s, 1H, *exch*, NH), 12.95 (s, 1H, *exch*, COOH); Anal. calcd. for

(C₁₄H₁₃N₅O₄S · 0.1Acetone · 2.55H₂O) C, H, N, S; UPLC-MS > 95%; m/z [M+H]⁺, calcd 348.07, found 348.21.

5-[[N-methyl-(2-amino-4-oxo-4,7-dihydro-3H-pyrrolo[2,3-*d*]pyrimidin-6-yl)-methylamino]-carbonyl]-thiophene-3-carboxylic acid (28e)

Compound **28e** was synthesized in 78% yield following the procedure of **28a**. mp > 250 °C; TLC *R_f* 0.51 (CHCl₃: MeOH: AcOH, 10:1:0.5); ¹H NMR (DMSO-*d*₆) δ 2.95 (s, 3H, *cis* and *trans* NCH₃), 4.45-4.54 (d, 2H, *cis* and *trans* NCH₂), 6.07 (s, 2H, *exch*, 2-NH₂), 6.13 (s, 1H, *cis* and *trans* 5-H), 7.81 (s, 1H, thiophene), 8.17 (s, 1H, thiophene), 10.24 (s, 1H, *exch*, NH), 10.98 (s, 1H, *exch*, NH), 13.35 (s, 1H, *exch*, COOH); Anal. calcd. for (C₁₄H₁₃N₅O₄S · 1.06H₂O) C, H, N, S; UPLC-MS > 95%; m/z [M+H]⁺, calcd 348.07, found 348.24.

4-[[N-methyl-(2-amino-4-oxo-4,7-dihydro-3H-pyrrolo[2,3-*d*]pyrimidin-6-yl)-methylamino]-sulfonyl]-phenylcarboxylic acid (28f)

Compound **28f** was synthesized in 91% yield following the procedure of **28a**. mp > 250 °C; TLC *R_f* 0.45 (CHCl₃: MeOH: AcOH, 10:1:0.5); ¹H NMR (DMSO-*d*₆) δ 2.57 (s, 3H, NCH₃), 4.12 (s, 2H, NCH₂), 6.69 (s, 1H, 5-H), 6.78 (s, 2H, *exch*, 2-NH₂), 7.92 (d, *J* = 7.6 Hz, 2H, Ph), 8.15 (d, *J* = 7.6 Hz, 2H, Ph), 10.87 (s, 1H, *exch*, NH), 11.48 (s, 1H, *exch*, NH), 13.50 (br, 1H, *exch*, COOH); UPLC-MS > 95%; m/z [M+H]⁺, calcd 378.08, found 378.26.

General procedures for the synthesis of 29a-f

To a solution of **28a-f** (1 eq.) in DMF (1 mL) were added *N*-methyl morpholine (3 eq.) and 2-chloro-4,6-dimethoxy-1,3,5-triazine (1.05 eq.). The mixture was stirred at rt for 1 h. Dimethyl L-glutamate (1.1 eq.) was added and the mixture was stirred overnight. The solvent was evaporated and the residue was purified

by a silica column with chloroform and methanol to give **29a-f**. Compounds **29a-f** were directly used in the next step reaction without identification.

General procedures for the synthesis of 7-12

To a solution of **29a-f** (1.0 eq.) in water (10 mL) and methanol (10 mL) was added Na₂CO₃ (0.5 g). The mixture was stirred at 80 °C rt. Methanol was removed and the mixture was adjusted to pH 3 with 1N HCl. The suspension was filtered and the filter cake was washed with deionized water, and acetone to facilitate the drying process. The resulting solid was dried at 50 °C in vacuum overnight to afford a white solid **7-12**.

(S)-2-(4-([N-Methyl-(2-amino-4-oxo-4,7-dihydro-3H-pyrrolo[2,3-*d*]pyrimidin-6-yl)-methylamino]-carbonyl)-phenyl-1-carbonyl)amino pentanedioic acid (7)

Yield: 64%. TLC *R_f* 0.12 (CHCl₃/MeOH/AcOH, 10:1:0.1); mp > 250 °C; ¹H NMR (DMSO-*d*₆) δ 1.94 (m, 1H, CH₂), 2.09 (m, 1H, CH₂), 2.35 (t, *J* = 7.6 Hz, 2H, CH₂), 2.81 (s, 1.8H, *cis* NCH₃), 2.94 (s, 1.2H, *trans* NCH₃), 4.31 (s, 0.8H, *trans* NCH₂), 4.41 (s, 1.2H, *cis* NCH₂), 4.59 (m, 1H, CH), 6.02 (s, 0.4H, *trans* 5-H), 6.08 (s, 2H, *exch*, 2-NH₂), 6.17 (s, 0.6H, *cis* 5-H), 7.55 (d, *J* = 6.4 Hz, 2H, Ph), 7.93 (d, *J* = 6.4 Hz, 2H, Ph), 8.71 (s, 1H, *exch*, CONH), 10.23 (s, 1H, *exch*, NH), 11.02 (s, 1H, *exch*, NH), 12.59 (br, 2H, *exch*, COOH); Anal. calcd. for (C₂₁H₂₂N₆O₇ · 0.95H₂O) C, H, N; UPLC-MS > 95%; *m/z* [M+H]⁺, calcd 471.16, found 471.26.

(S)-2-(3-([N-methyl-(2-amino-4-oxo-4,7-dihydro-3H-pyrrolo[2,3-*d*]pyrimidin-6-yl)-methylamino]-carbonyl)phenylcarbonyl)amino pentanedioic acid (8)

Yield: 56%. TLC *R_f* 0.18 (CHCl₃/MeOH/AcOH, 10:1:0.1); mp > 250 °C; ¹H NMR (DMSO-*d*₆) δ 1.99 (m, 1H, CH₂), 2.09 (m, 1H, CH₂), 2.33 (m, 2H, CH₂), 2.81 (s, 1.5H, *cis* NCH₃), 2.93 (s, 1.5H, *trans* NCH₃), 4.32 (s, 1.0H, *trans* NCH₂), 4.32 (s, 1.0H, *cis* NCH₂), 4.60 (m, 1H, CH), 5.93 (s, 0.5H, *trans* 5-H), 6.06 (s, 2H, *exch*, 2-NH₂), 6.17 (s, 0.5H, *cis* 5-H), 7.54 (m, 1H, Ph), 7.61 (m, 1H, Ph), 7.96 (m, 2H), 8.61 (s, 1H,

exch, CONH), 10.09 (s, 1H, exch, NH), 10.23 (s, 1H, exch, NH), 11.05 (br, 1H, exch, COOH), 11.13 (br, 1H, exch, COOH); UPLC-MS > 95%; m/z [M+H]⁺, calcd 471.16, found 471.26.

(S)-2-(5-([N-methyl-(2-amino-4-oxo-4,7-dihydro-3H-pyrrolo[2,3-d]pyrimidin-6-yl)-methylamino]-carbonyl)-thiophene-2-carbonyl)amino pentanedioic acid (9)

Yield: 61%. TLC *R_f* 0.19 (CHCl₃/MeOH/AcOH, 10:1:0.5); mp > 250 °C; ¹H NMR (DMSO-d₆) δ 1.91 (q, J = 7.2 Hz, 2H, CH₂), 2.35 (t, J = 6.8 Hz, 2H, CH₂), 3.11 (br, 3H, *cis and trans* NCH₃), 4.40 (q, J = 9.6 Hz, 1H, CH), 4.58 (s, 2H, *cis and trans* NCH₂), 6.09 (s, 2H, exch, 2-NH₂), 6.12 (s, 1H, *cis and trans* 5-H), 7.51 (d, J = 7.2 Hz, 1H, thiophene), 7.82 (d, J = 6.4 Hz, 1H, thiophene), 8.81 (d, J = 2.0 Hz, 1H, exch, CONH), 10.25 (s, 1H, exch, NH), 11.04 (s, 1H, exch, NH), 12.27 (s, 1H, exch, COOH), 12.82 (s, 1H, exch, COOH); Anal. calcd. for (C₁₉H₂₀N₆O₇S · 0.2Acetone · 1.16H₂O) C, H, N, S; UPLC-MS > 95%; m/z [M+H]⁺, calcd 477.11, found 477.16.

(S)-2-(4-([N-methyl-(2-amino-4-oxo-4,7-dihydro-3H-pyrrolo[2,3-d]pyrimidin-6-yl)-methylamino]-carbonyl)-thiophene-2-carbonyl) amino pentanedioic acid (10)

Yield: 70%. TLC *R_f* 0.15 (CHCl₃/MeOH/AcOH, 10:1:0.5); mp > 250 °C; ¹H NMR (DMSO-d₆) δ 1.90 (m, 1H, CH₂), 2.07 (m, 1H, CH₂), 2.34 (t, J = 7.6 Hz, 2H, CH₂), 3.12 (s, 3H, *cis and trans* NCH₃), 4.36 (q, J = 7.6 Hz, 1H, CH), 4.54 (s, 2H, *cis and trans* NCH₂), 6.08 (s, 2H, exch, 2-NH₂), 6.12 (s, 1H, *cis and trans* 5-H), 7.86 (s, 1H, thiophene), 8.38 (m, 1H, thiophene), 8.56 (d, J = 7.6 Hz, 1H, exch, CONH), 10.24 (s, 1H, exch, NH), 11.04 (s, 1H, exch, NH), 12.27 (br, 1H, exch, COOH), 12.70 (br, 1H, exch, COOH); Anal. calcd. for (C₁₉H₂₀N₆O₇S · 0.45Acetone · 1.83H₂O) C, H, N, S; UPLC-MS > 95%; m/z [M+H]⁺, calcd 477.11, found 477.22.

(S)-2-(5-([N-methyl-(2-amino-4-oxo-4,7-dihydro-3H-pyrrolo[2,3-d]pyrimidin-6-yl)-methylamino]-carbonyl)-thiophene-3-carbonyl)amino pentanedioic acid (11)

Yield: 74%. TLC *R_f* 0.19 (CHCl₃/MeOH/AcOH, 10:1:0.5); mp > 250 °C; ¹H NMR (DMSO-d₆) δ 1.92 (m, 1H, CH₂), 2.09 (m, 1H, CH₂), 2.35 (m, 2H, CH₂), 3.01 (s, 3H, *cis and trans* NCH₃), 4.35 (m, 1H, CH), 4.54 (s, 2H, *cis and trans* NCH₂), 6.08 (s, 2H, *exch*, 2-NH₂), 6.12 (s, 1H, *cis and trans* 5-H), 7.96 (s, 1H, thiophene), 8.07 (s, 1H, thiophene), 8.79 (d, *J* = 1.2 Hz, 1H, *exch*, CONH), 10.24 (s, 1H, *exch*, NH), 11.00 (s, 1H, *exch*, NH), 12.27 (br, 1H, *exch*, COOH), 12.69 (s, 1H, *exch*, COOH); Anal. calcd. for (C₁₉H₂₀N₆O₇S·1.77H₂O) C, H, N, S; UPLC-MS > 95%; *m/z* [M+H]⁺, calcd 477.11, found 477.26.

(S)-2-(4-[[*N*-methyl-(2-amino-4-oxo-4,7-dihydro-3H-pyrrolo[2,3-*d*]pyrimidin-6-yl)-methyldamino]-sulfonyl]-phenylcarbonyl)amino pentanedioic acid (12)

Yield: 60%. TLC *R_f* 0.17 (CHCl₃/MeOH/AcOH, 10:1:0.5); mp 239.3 - 241.7 °C; ¹H NMR (DMSO-d₆) δ 1.98 (m, 1H, CH₂), 1.99 (m, 1H, CH₂), 2.38 (t, *J*=8.0 Hz, 2H, CH₂), 3.38 (s, 3H, NCH₃), 4.06 (s, 2H, NCH₂), 4.44 (m, 1H, CH), 6.11 (s, 2H, *exch*, 2-NH₂), 6.12 (s, 1H, 5-H), 7.95 (d, *J* = 8.0 Hz, 2H, Ph), 8.13 (d, *J* = 8.0 Hz, 2H, Ph), 8.92 (d, *J* = 1.2 Hz, 1H, *exch*, CONH), 10.24 (s, 1H, *exch*, NH), 11.11 (s, 1H, *exch*, NH), 12.16 (br, 1H, *exch*, COOH), 12.69 (br, 1H, *exch*, COOH); Anal. calcd. for (C₂₀H₂₂N₆O₈S·0.5Acetone·0.92H₂O) C, H, N, S; UPLC-MS > 95%; *m/z* [M+H]⁺, calcd 507.12, found 507.20.

Molecular modeling and computational studies

Molecular modeling was performed for all analogs with the FRα (PDB: 5IZQ) and GARFTase (PDB: 4ZZ1) crystal structures using the induced fit docking protocol of Maestro.⁴⁹ The ligands were prepared using the Ligprep application of Maestro. The docking protocol was validated by re-docking the co-crystallized ligands **6** (FRα) and **3** (GARFTase) into the crystal structures with RMSD values of 0.15 Å and 0.23 Å, respectively. The centroid around the ligands were defined as the ligand binding site. The OPLS3e force field was used and amino acid residues within 5 Å from the docked poses were allowed to be optimized using prime refinement. Using prepared ligands from the Ligprep files, we used Conformational Search (Macromodel) to determine the number of low energy conformations within 5 kcal/mol from the minimum

energy conformation; the settings were as follows: Force Field, OPLS3e; Solvent, water; Conformation Search Method, Mixed Torsional/Low-Mode sampling (the remaining settings were set default).

Reagents for biological studies. [$^{14}\text{C}(\text{U})$]Glycine (87 mCi/mmol) was purchased from Moravsek Biochemicals (Brea, CA). Unlabeled folic acid was purchased from the Sigma Chemical Co. (St. Louis, MO). Leucovorin [(6R,S) 5-formyl tetrahydrofolate] was provided by the Drug Development Branch, National Cancer Institute, Bethesda, MD. The sources of the classical antifolate drugs were as follows: MTX, Drug Development Branch, National Cancer Institute (Bethesda, MD); RTX [*N*-(5-[*N*-(3,4-dihydro-2-methyl-4-oxyquinazolin-6-ylmethyl)-*N*-methyl-amino]-2-thienoyl)- L-glutamic acid], AstraZeneca Pharmaceuticals (Macclesfield, Cheshire, England); and PMX [*N*-(4-[2-(2-amino-3,4-dihydro-4-oxo-7H-pyrrolo[2,3-*d*]pyrimidin-5-yl)ethyl]benzoyl)- L-glutamic acid] (Alimta) (LC Laboratories, Woburn, MA). Other chemicals were obtained from commercial sources in the highest available purity.

Cell culture. MTXR^{II}Oua^R2-4 (hereafter, referred to as R2) is a RFC-, PCFT- and FR α -null CHO cell line⁴⁵ that was a gift from Dr. Wayne Flintoff (University of Western Ontario). From this parental cell line, RFC, PCFT and FR α were transfected to generate isogenic CHO cell lines designated PC43-10 (expresses human RFC but not PCFT or FR α), R2/PCFT4 (expresses human PCFT), and RT16 (expresses human FR α).^{23,24,44} The CHO sublines were maintained in α -minimal essential medium (α -MEM) supplemented with 1% penicillin-streptomycin solution, 2 mM L-glutamine and 10% heat-treated bovine calf serum (Invitrogen). Transfected cell lines were cultured with 1 mg/ml G418. FR-expressing CHO cell lines were cultured for 72 hours prior to cell viability experiments in folate-free RPMI 1640 (FF-RPMI) (Invitrogen) with 10% dialyzed fetal bovine serum (dFBS) (Invitrogen), supplemented with 1% penicillin-streptomycin and L-glutamine. Human KB carcinoma cells were purchased from ATCC (Manassas, VA) continuously maintained in complete FF-RPMI with 10% fetal bovine serum and 1% penicillin-streptomycin and L-glutamine.

Cell proliferation assays were performed exactly as previously described.^{23,25,27,28,33,34,36,44} Cell lines were treated with a range of concentrations of standard or novel inhibitors (0-1000 nM) in a 96 well plate with FF-RPMI complete and 10% dFBS, supplemented with 2 nM (RT-16, D4, KB) or 25 nM (R2/PCFT4, R2, PC43-10) leucovorin, 1% penicillin–streptomycin and L-glutamine (2 mM), over a 96 h incubation period at 37 °C with 5% CO₂. To confirm FR-mediated drug uptake and growth inhibition, 200 nM folic acid was added to parallel incubations with drug. To quantitate viable cells, the media was removed and Cell Titer-blue™ reagent (Promega) was added. Relative cell numbers were determined by fluorescence measurements with a fluorescence plate reader (Molecular Devices) at 590 nm emission and 560 nm excitation. IC₅₀ values, corresponding to drug concentrations that resulted in 50% loss of cell growth, were calculated from dose-response curves using Sigma Plot (v.12) software.

In order to identify the targeted pathways/folate-dependent enzymes by the classic and novel pyrrolo[2,3-*d*]pyrimidine antifolates, proliferation assays were performed with KB cell cultured in complete glycine free FF-RPMI with dFBC in the presence of adenosine (60 µM), thymidine (10 µM), glycine (130 µM) or AICA hydrochloride (320 µM); results were compared to incubations in parallel without nucleoside/AICA or drug additions.

***In situ* GARFTase inhibition assays.** To measure the extent of intracellular GARFTase inhibition in the presence of antifolate inhibitors, we measured the metabolic incorporation of [¹⁴C(U)] glycine into [¹⁴C]formyl GAR in the presence of azaserine.^{23-25,27,28,33,34,36,44,50} KB cells were seeded in complete media (above) and allowed to adhere to the substratum for 24 h. Cells were washed with FF-RPMI, L- glutamine free with 10% dFBS, 1% penicillin-streptomycin and 2 nM LCV. Cells were incubated at 37° C with 5% CO₂ for 1 h with folate- and L-glutamine-depleted media containing 2 nM LCV with the antifolate compounds over a range of concentrations. Control cells were treated with an equal volume of DMSO. Azaserine (4 µM final concentration) was added to the cells and cells were incubated for 30 minutes. This was followed by the addition of L-glutamine (2 mM) and [¹⁴C(U)]glycine (final specific activity 0.1 mCi/L).

Cells were incubated for an additional 16 h, then washed with ice-cold DPBS, trypsinized and collected. Cells were treated with 5% trichloroacetic acid (TCA) at 0°C. Samples were centrifuged (4°C, 14,000 rpm) and the protein precipitants were solubilized with 0.5 N NaOH for quantitation of protein concentrations with the Folin-phenol protein method.⁵¹ The TCA supernatants were extracted with cold ether. After evaporation of ether, the remaining aqueous layer was gravity filtered through a 1 cm chromatography column (Bio-rad) of AG1x8 (chloride form). The columns were washed with 10 mL each of 0.5 N formic acid, followed by 4 N formic acid and finally eluted with 8 ml of 1 N HCl collected in 8 one ml fractions. The eluate was measured for radioactivity and the percentages of radioactivity in the [¹⁴C]formyl GAR and non-specific [¹⁴C]fractions determined. The results were calculated as pmol [¹⁴C]formyl GAR/mg protein. The data were plotted using Sigmaplot (v.12) and the IC₅₀s were calculated for the drug-treated samples, compared to the untreated controls.

ACKNOWLEDGMENTS

This work was supported in part by grants from the National Institutes of Health R01 CA53535 (LHM and ZH), R01 CA125153 (AG), R01 CA152316 (LHM and AG), and R01 CA166711 (AG, LHM and CED), the Eunice and Milton Ring Endowed Chair for Cancer Research (LHM), and the Duquesne University Adrian Van Kaam Chair in Scholarly Excellence (AG).

References

1. Matherly LH, Wilson MR, Hou Z. The major facilitative folate transporters solute carrier 19A1 and solute carrier 46A1: biology and role in antifolate chemotherapy of cancer. *Drug Metab Dispos.* 2014;42:632-649.
2. Visentin M, Zhao R, Goldman ID. The Antifolates. *Hematol Oncol Clin N.* 2012;26(3):629-ix.
3. Matherly LH, Hou Z, Deng Y. Human reduced folate carrier: translation of basic biology to cancer etiology and therapy. *Cancer Metastasis Rev.* 2007;26:111-128.
4. Kugel Desmoulin S, Wang L, Polin L, et al. Functional loss of the reduced folate carrier enhances the antitumor activities of novel antifolates with selective uptake by the proton-coupled folate transporter. *Mol Pharmacol.* 2012;82:591-600.
5. Matherly LH, Hou Z, Gangjee A. The promise and challenges of exploiting the proton-coupled folate transporter for selective therapeutic targeting of cancer. *Cancer Chemother Pharmacol.* 2018;81:1-15.

6. Zhao R, Min SH, Qiu A, et al. The spectrum of mutations in the PCFT gene, coding for an intestinal folate transporter, that are the basis for hereditary folate malabsorption. *Blood*. 2007;110:1147-1152.
7. Zhao R, Goldman ID. The proton-coupled folate transporter: physiological and pharmacological roles. *Curr Opin Pharmacol*. 2013;13(6):875-880.
8. Elnakat H, Ratnam M. Distribution, functionality and gene regulation of folate receptor isoforms: implications in targeted therapy. *Adv Drug Deliv Rev*. 2004;56:1067-1084.
9. Xia W, Low PS. Folate-targeted therapies for cancer. *J Med Chem*. 2010;53(19):6811-6824.
10. Cherian C, Kugel Desmoulin S, Wang L, et al. Therapeutic targeting malignant mesothelioma with a novel 6-substituted pyrrolo[2,3-d]pyrimidine thienoyl antifolate via its selective uptake by the proton-coupled folate transporter. *Cancer Chemother Pharmacol*. 2013;71:999-1011.
11. Hou Z, Gattoc L, O'Connor C, et al. Dual targeting of epithelial ovarian cancer via folate receptor alpha and the proton-coupled folate transporter with 6-substituted pyrrolo[2,3-d]pyrimidine antifolates. *Mol Cancer Ther*. 2017;16:819-830.
12. Wilson MR, Hou Z, Yang S, et al. Targeting Nonsquamous Nonsmall Cell Lung Cancer via the Proton-Coupled Folate Transporter with 6-Substituted Pyrrolo[2,3-d]Pyrimidine Thienoyl Antifolates. *Mol Pharmacol*. 2016;89:425-434.
13. Giovannetti E, Zucali PA, Assaraf YG, et al. Role of proton-coupled folate transporter in pemetrexed-resistance of mesothelioma: clinical evidence and new pharmacological tools. *Ann Oncol*. 2017;28:2725-2732.
14. Desmoulin SK, Hou Z, Gangjee A, Matherly LH. The human proton-coupled folate transporter: Biology and therapeutic applications to cancer. *Cancer Biol Ther*. 2012;13:1355-1373.
15. Parker N, Turk MJ, Westrick E, Lewis JD, Low PS, Leamon CP. Folate receptor expression in carcinomas and normal tissues determined by a quantitative radioligand binding assay. *Anal Biochem*. 2005;338:284-293.
16. Kamen BA, Smith AK. Farletuzumab, an anti-folate receptor alpha antibody, does not block binding of folate or anti-folates to receptor nor does it alter the potency of anti-folates in vitro. *Cancer Chemother Pharmacol*. 2012;70(1):113-120.
17. Armstrong DK, White AJ, Weil SC, Phillips M, Coleman RL. Farletuzumab (a monoclonal antibody against folate receptor alpha) in relapsed platinum-sensitive ovarian cancer. *Gynecologic oncology*. 2013;129(3):452-458.
18. Kurkjian C, LoRusso, P., Sankhala, K.K., Birrer, M.J., Kirby, M., Ladd, S., Hawes, S., Running, K.L., O'Leary, J.J., Moore, K.N. A phase I, first-in-human study to evaluate the safety, pharmacokinetics (PK), and pharmacodynamics (PD) of IMGN853 in patients (Pts) with epithelial ovarian cancer (EOC) and other FOLR1-positive solid tumors. *J Clin Oncol* 2013;31 (15 Suppl.):2573.
19. Assaraf YG, Leamon CP, Reddy JA. The folate receptor as a rational therapeutic target for personalized cancer treatment. *Drug Resist Updat*. 2014;17(4-6):89-95.
20. Gibbs DD, Theti DS, Wood N, et al. BGC 945, a novel tumor-selective thymidylate synthase inhibitor targeted to alpha-folate receptor-overexpressing tumors. *Cancer Res*. 2005;65(24):11721-11728.
21. Leamon CP, Jackman AL. Exploitation of the folate receptor in the management of cancer and inflammatory disease. *Vitam Horm*. 2008;79:203-233.
22. Udai Banerji AHIG, Vasiliki Michalarea, Ruth Ruddle, Florence I. Raynaud, Ruth Riisnaes, Daniel Nava Rodrigues, Nina Tunariu, Joanna C Porter, Sarah Emily Ward, Mona Parmar, Alison Joanne Turner, Satyanarayana Seeramreddi, Emma Hall, Emma Jane Dean, Bristi Basu, Angela George, Stan B Kaye, Susana N. Banerjee, Johann S. De Bono An investigator-initiated phase I study of

- ONX-0801, a first-in-class alpha folate receptor targeted, small molecule thymidylate synthase inhibitor in solid tumors. *J Clin Oncol.* 2017; 35 (15 suppl):2503.
23. Deng Y, Wang Y, Cherian C, et al. Synthesis and discovery of high affinity folate receptor-specific glycinamide ribonucleotide formyltransferase inhibitors with antitumor activity. *J Med Chem.* 2008;51:5052-5063.
 24. Kugel Desmoulin S, Wang Y, Wu J, et al. Targeting the proton-coupled folate transporter for selective delivery of 6-substituted pyrrolo[2,3-d]pyrimidine antifolate inhibitors of de novo purine biosynthesis in the chemotherapy of solid tumors. *Mol Pharmacol.* 2010;78:577-587.
 25. Wang L, Kugel Desmoulin S, Cherian C, et al. Synthesis, biological, and antitumor activity of a highly potent 6-substituted pyrrolo[2,3-d]pyrimidine thienoyl antifolate inhibitor with proton-coupled folate transporter and folate receptor selectivity over the reduced folate carrier that inhibits beta-glycinamide ribonucleotide formyltransferase. *J Med Chem.* 2011;54:7150-7164.
 26. Wang L, Wallace A, Raghavan S, et al. 6-Substituted Pyrrolo[2,3-d]pyrimidine Thienoyl Regioisomers as Targeted Antifolates for Folate Receptor α and the Proton-Coupled Folate Transporter in Human Tumors. *J Med Chem.* 2015;58(17):6938-6959.
 27. Golani LK, Wallace-Povirk A, Deis SM, et al. Tumor Targeting with Novel 6-Substituted Pyrrolo [2,3-d] Pyrimidine Antifolates with Heteroatom Bridge Substitutions via Cellular Uptake by Folate Receptor alpha and the Proton-Coupled Folate Transporter and Inhibition of de Novo Purine Nucleotide Biosynthesis. *J Med Chem.* 2016;59(17):7856-7876.
 28. Golani LK, George C, Zhao S, et al. Structure-activity profiles of novel 6-substituted pyrrolo[2,3-d]pyrimidine thienoyl antifolates with modified amino acids for cellular uptake by folate receptors alpha and beta and the proton-coupled folate transporter. *J Med Chem.* 2014;57(19):8152-8166.
 29. Laursen JS, Engel-Andreasen J, Fristrup P, Harris P, Olsen CA. Cis–Trans Amide Bond Rotamers in β -Peptoids and Peptoids: Evaluation of Stereoelectronic Effects in Backbone and Side Chains. *J Am Chem Soc.* 2013;135(7):2835-2844.
 30. Sliwoski G, Kothiwale S, Meiler J, Lowe EW. Computational Methods in Drug Discovery. *Pharmacol Rev.* 2014;66(1):334-395.
 31. Szostak M, Aubé J. The Chemistry of Bridged Lactams and Related Heterocycles. *Chem Rev.* 2013;113(8):5701-5765.
 32. Chen P, Feng D, Qian X, et al. Structure-activity-relationship of amide and sulfonamide analogs of omarigliptin. *Bioorganic & medicinal chemistry letters.* 2015;25(24):5767-5771.
 33. Wang L, Cherian C, Kugel Desmoulin S, et al. Synthesis and antitumor activity of a novel series of 6-substituted pyrrolo[2,3-d]pyrimidine thienoyl antifolate inhibitors of purine biosynthesis with selectivity for high affinity folate receptors and the proton-coupled folate transporter over the reduced folate carrier for cellular entry. *J Med Chem.* 2010;53:1306-1318.
 34. Wang L, Wallace A, Raghavan S, et al. 6-Substituted Pyrrolo[2,3-d]pyrimidine Thienoyl Regioisomers as Targeted Antifolates for Folate Receptor alpha and the Proton-Coupled Folate Transporter in Human Tumors. *J Med Chem.* 2015;58(17):6938-6959.
 35. Li X, Liu S, Huang H, et al. Gambogic Acid Is a Tissue-Specific Proteasome Inhibitor In Vitro and In Vivo. *Cell Reports.* 2013;3(1):211-222.
 36. Wang L, Cherian C, Kugel Desmoulin S, et al. Synthesis and Biological Activity of 6-Substituted Pyrrolo[2,3-d]pyrimidine Thienoyl Regioisomers as Inhibitors of de Novo Purine Biosynthesis with Selectivity for Cellular Uptake by High Affinity Folate Receptors and the Proton-Coupled Folate Transporter over the Reduced Folate Carrier. *J Med Chem.* 2012;55(4):1758-1770.
 37. Proctor LD, Warr AJ. Development of a Continuous Process for the Industrial Generation of Diazomethane. *Org Process Res Dev.* 2002;6(6):884-892.

38. Akimoto H, Imamiya E, Hitaka T, Nomura H, Nishimura S. Synthesis of queuine, the base of naturally occurring hypermodified nucleoside (queuosine), and its analogues. *Journal of the Chemical Society, Perkin Transactions 1*. 1988(7):1637-1644.
39. Gangjee A, Mavandadi F, Kisliuk RL, Queener SF. Synthesis of Classical and a Nonclassical 2-Amino-4-oxo-6-methyl-5-substituted Pyrrolo[2,3-d]pyrimidine Antifolate Inhibitors of Thymidylate Synthase. *J Med Chem*. 1999;42(12):2272-2279.
40. Linz S, Troschuetz R. Synthesis of 5-[(4-phenylpiperazin-1-yl)methyl]pyrrolo[2,3-d]pyrimidine derivatives as potential dopamine D4 receptor ligands. *J Heterocycl Chem*. 2007;44(2):349-354.
41. Seela F, Chen Y, Zulauf M. Regioselectivity of the Mannich reaction on pyrrolo[2,3-d]pyrimidine nucleosides related to 7-deaza-2'-deoxyadenosine or 7-deaza-2'-deoxyguanosine. *Synthese*. 1997(9):1067-1072.
42. Xiang W, Choudhary S, Hamel E, Mooberry SL, Gangjee A. Structure based drug design and in vitro metabolism study: Discovery of N-(4-methylthiophenyl)-N,2-dimethyl-cyclopenta[d]pyrimidine as a potent microtubule targeting agent. *Bioorganic & medicinal chemistry*. 2018;26(9):2437-2451.
43. Quintanilla-Licea R, Colunga-Valladares J, Caballero-Quintero A, et al. NMR Detection of Isomers Arising from Restricted Rotation of the C-N Amide Bond of N-Formyl-o-toluidine and N,N'-bis-Formyl-o-toluidine. *Molecules*. 2002;7(8):662.
44. Deng Y, Zhou X, Kugel Desmoulin S, et al. Synthesis and biological activity of a novel series of 6-substituted thieno[2,3-d]pyrimidine antifolate inhibitors of purine biosynthesis with selectivity for high affinity folate receptors over the reduced folate carrier and proton-coupled folate transporter for cellular entry. *J Med Chem*. 2009;52:2940-2951.
45. Flintoff WF, Nagainis CR. Transport of methotrexate in Chinese hamster ovary cells: a mutant defective in methotrexate uptake and cell binding. *Arch Biochem Biophys*. 1983;223:433-440.
46. Mitchell-Ryan S, Wang Y, Raghavan S, et al. Discovery of 5-Substituted Pyrrolo[2,3-d]pyrimidine Antifolates as Dual-Acting Inhibitors of Glycinamide Ribonucleotide Formyltransferase and 5-Aminoimidazole-4-carboxamide Ribonucleotide Formyltransferase in De Novo Purine Nucleotide Biosynthesis: Implications of Inhibiting 5-Aminoimidazole-4-carboxamide Ribonucleotide Formyltransferase to AMPK Activation and Antitumor Activity. *J Med Chem*. 2013;56(24):10016-10032.
47. Ducker GS, Ghergurovich JM, Mainolfi N, et al. Human SHMT inhibitors reveal defective glycine import as a targetable metabolic vulnerability of diffuse large B-cell lymphoma. *Proc Natl Acad Sci U S A*. 2017;114(43):11404-11409.
48. Taylor EC, Kuhnt D, Shih C, et al. A dideazatetrahydrofolate analog lacking a chiral center at C-6: N-[4-[2-(2-amino-3,4-dihydro-4-oxo-7H-pyrrolo[2,3-d]pyrimidin-5yl)ethyl]benzoyl]-L-glutamic acid is an inhibitor of thymidylate synthase. *J Med Chem*. 1992;35(23):4450-4454.
49. Saez-Calvo G, Sharma A, Balaguer FA, et al. Triazolopyrimidines Are Microtubule-Stabilizing Agents that Bind the Vinca Inhibitor Site of Tubulin. *Cell Chem Biol*. 2017;24(6):737-750 e736.
50. Kugel Desmoulin S, Wang L, Hales E, et al. Therapeutic targeting of a novel 6-substituted pyrrolo [2,3-d]pyrimidine thienoyl antifolate to human solid tumors based on selective uptake by the proton-coupled folate transporter. *Mol Pharmacol*. 2011;80:1096-1107.
51. Lowry OH, Rosebrough NJ, Farr AL, Randall RJ. Protein measurement with the Folin phenol reagent. *The Journal of biological chemistry*. 1951;193(1):265-275.